Cell Death Discovery

https://doi.org/10.1038/s41420-026-02980-9

Article in Press

Targeting integrin beta 4 in diacetyl-induced anoikis of the airway epithelium

Received: 29 August 2025

Revised: 28 December 2025

Accepted: 16 February 2026

Cite this article as: Kim, S.-Y., Pitonzo, A., Huyck, H. *et al.* Targeting integrin beta 4 in diacetyl-induced anoikis of the airway epithelium. *Cell Death Discov.* (2026). https://doi.org/10.1038/s41420-026-02980-9

So-Young Kim, Ariana Pitonzo, Heidie Huyck, Gloria S. Pryhuber, Thomas J. Mariani & Matthew D. McGraw

Targeting Integrin Beta 4 in Diacetyl-Induced Anoikis of the Airway Epithelium

So-Young Kim, MS[1,2], Ariana Pitonzo[3], Heidie Huyck[3], Gloria S. Pryhuber, MD[2,3], Thomas J. Mariani, PhD[2,3] & Matthew D. McGraw, MD[1,2]*

Affiliations: [1]Department of Pediatrics, Division of Pediatric Pulmonology; [2]Department of Environmental Medicine, [3]Department of Pediatrics, Division of Neonatology; University of Rochester Medical Center, Rochester, NY 14642, USA.

Running Head: Integrin beta 4 in diacetyl-induced anoikis

Keywords: diacetyl; anoikis; lung; airway epithelium; bronchiolitis obliterans

***Corresponding Author:**
Matthew D. McGraw, MD
University of Rochester Medical Center
Dept. of Pediatrics, Div. of Pulmonology
601 Elmwood Avenue, Box 667, Rochester, NY 14642
matthew_mcgraw@urmc.rochester.edu
Phone: (585) 275-2464; Fax: (585) 275-8706

Abstract

Diacetyl (DA) is a flavoring chemical commonly found in food and beverages. When inhaled at occupationally-relevant concentrations, DA can cause bronchiolitis obliterans (BO), yet the mechanisms remain poorly understood. Common to all forms of BO is airway epithelial injury with failed epithelial cell survival contributing to BO development. The purpose of the current study was to target integrin beta 4 (ITGβ4) – one of the primary integrins that connect airway epithelial cells to the basement membrane – in DA-exposed airway epithelial cells to prevent adhesion-related cell apoptosis ('anoikis'). Sprague-Dawley rats were exposed to 200 parts-per-million DA vapor or filtered air for 6 hours per day for 5 consecutive days, then monitored for 5 weeks post-exposure and assessed for airway remodeling using Trichrome staining and the hydroxyproline assay. ITGβ4 protein expression was assessed via western blot as well as co-immunofluorescent staining using common airway epithelial cell markers. In parallel, primary human airway epithelial cells and human bronchial epithelial cells (16HBE14o-) were grown *in vitro*, exposed to DA, and treated with the pan-caspase inhibitor Z-VAD-FMK or transfected with ITGB4. End-points included viability staining, extracellular caspase 3/7 activity and ITGβ4 protein expression. Rats exposed to DA vapors developed significant airway remodeling with increased total lung collagen content and sub-epithelial airway collagen deposition. Airway epithelial ITGβ4 expression remained decreased weeks after DA exposure with expansion of pan-cytokeratin positive epithelial cells, independent of ciliated and club cell markers. In parallel, DA-exposed human airway epithelial cells exposed *in vitro* developed significant anoikis. Treatment with Z-VAD-FMK reduced anoikis and improved ITGβ4 cytoplasmic surface expression but failed to improve total ITGβ4 protein expression. ITGB4 overexpression failed to suppress ITGβ4 cleavage nor prevent anoikis. In

summary, DA exposure in both rats and human airway epithelial cells results in caspase-mediated cleavage of ITGβ4. Future studies targeting post-translational modifications of ITGβ4 may prevent airway epithelial cell anoikis and fibrotic remodeling.

1. Introduction

Diacetyl (DA) (2,3-butanedione) is a chemical often added or naturally occurring in food and drinks for its buttery flavor (1). DA is an alpha (α)-diketone with a low boiling point and high vapor pressure. Inherent of its chemical properties, DA is volatile often existing as a vapor (2). While DA is generally recognized as safe (GRAS) for consumption by the United States' Food & Drug Administration (FDA), many countries, including the United Kingdom and Canada, have restricted or banned its use. In support of this ban, workers exposed to high concentrations of DA vapors for extended periods of time have developed the debilitating, fibrotic lung disease of bronchiolitis obliterans (BO) (3, 4).

BO is a histopathologic diagnosis requiring lung biopsy (5). Due to the invasive nature of lung biopsy, few occupational workers exposed to DA undergo lung biopsy, making disease prevalence difficult to ascertain. In contrast, bronchiolitis obliterans syndrome (BOS) is a clinical diagnosis made using lung function testing as well as clinical signs and symptoms (5). Robust epidemiologic evaluations of workers exposed to high DA concentrations in microwave popcorn plants and coffee roasting facilities estimate the disease prevalence of BOS to be around 3% (6). Equally concerning, no FDA-approved medications are available for workers suffering from BOS. Hence, preclinical research that identifies novel targetable mechanisms for DA-induced BO remains important as a basis for therapeutic intervention.

Preclinical models of repetitive DA vapor exposures assist in understanding the complex mechanisms contributory to BO development (7, 8, 9, 10, 11). Rats exposed to DA vapors at occupationally relevant concentrations develop significant bronchial fibrosis with histopathology comparable to that seen in humans (7, 8, 9). A common histopathologic

feature in DA-exposed rodents is injury to the airway epithelium that precedes scar formation (12, 13). Following DA exposure, airway epithelial injury is shown with reduced acetylated tubulin and club cell secretory protein expression, two common airway epithelial cell markers, followed by sloughing and denudation of the airway epithelium (9). In mice exposed to DA at comparable concentrations, protein damage is marked by ubiquitin and sequestome-1 accumulation in intrapulmonary bronchial epithelium that co-localizes with keratin 8 and 18 (12). Higher magnification of DA-exposed airway epithelial cells using transmission electron microscopy also shows protein damage specific to club and ciliated cells (12, 13). These studies support DA inhalation injuring multiple airway epithelial cell types although other common airway epithelial cell types, including airway basal, serous, and neuroendocrine cells have not been evaluated (14, 15, 16). With time and increasing concentration, it is clear that DA-exposed airways develop severe remodeling with subepithelial extracellular matrix deposition and subsequent fibrosis around intrapulmonary bronchi (17), yet the mechanisms of failed airway repair remain inadequately mapped.

Most airway epithelial cells are connected to the adjacent basement membrane through hemidesmosomes (18). Hemidesmosomes are complex structures consisting of multiple interconnected proteins including plectin (PLEC), dystonin (DST), and integrins alpha 6 (ITGα6) and beta 4 (ITGβ4). The integrin pair of alpha 6 (ITGα6) and beta 4 (ITGβ4) are essential for maintaining the airway epithelium's connection to the adjacent basement membrane through matrix protein laminin 332. Internal to the cell, ITGβ4 pairs with plectin providing cytoskeletal stability via connection between these proteins and adjacent intermediate filaments including keratin 5 and 14 (18, 19). In our previous work, we

showed DA reacts directly with the intermediate filament keratin 5 (Krt5) resulting in non-reducing crosslink formation (11, 20). With higher DA concentrations, these protein cross-linkages persist in damaged airway epithelial cells, triggering downstream hemidesmosome instability (20). With time, this hemidesmosome instability results in reduced airway epithelial attachment to the adjacent basement membrane.

Considering integrin beta 4 spans the intercellular and extracellular compartments from epithelial cell to the basement membrane, we hypothesized that reduced surface expression of ITGβ4 is a sentinel, initiating event in late-onset, adhesion-related cell death, or ‘anoikis’, after DA exposure. To interrogate this hypothesis, ITGβ4 was overexpressed using plasmid transfection of ITGB4 and caspase-mediated cleavage inhibition using the small molecule Z-VAD-FMK to preserve airway epithelial attachment. We hypothesized that either ITGB4 overexpression or inhibition of caspase-mediated cleavage would prevent airway epithelial cell anoikis and in turn would promote airway epithelial recovery.

Results

Rats exposed to diacetyl vapors develop significant airway remodeling with increased lung collagen content and reduced ITGβ4 expression

Sprague-Dawley rats were exposed repetitively to occupationally-relevant concentrations of diacetyl (DA) vapors via whole body exposure and then monitored for up to 5 weeks post-exposure for airway remodeling (*Schematic Exposure*, **Figure 1A**). In line with prior publications (10, 21, 22), significant airway remodeling developed in DA-exposed rats versus air-exposed controls with increased airway collagen deposition shown by Trichrome staining (**Figure 1B**). Lung collagen content was semi-quantitated via the hydroxyproline assay. Consistent with Trichrome staining, lung collagen content was significantly increased in DA-exposed rat lungs versus air-exposed control lungs (**Figure 1C**).

Next, lungs were assessed for changes in integrin beta 4 (ITGβ4) protein expression at interval time points after DA exposure via western blot on lung homogenates (**Figure 1D & 1E**) and via immunofluorescent staining (**Figure 1E**). Rat lung ITGβ4 expression progressively decreased in DA-exposed lungs vs air-exposed controls. By immunofluorescent staining, normal airway epithelial cells positive for ITGβ4 connected to the airway basement membrane and were frequently found adjacent to intrapulmonary, immune cell aggregates (**Supplemental Figure S1**). In contrast, DA-exposed airways at 5 weeks post-DA exposure demonstrated reduced airway integrin beta 4 (ITGβ4) expression (**Figure 1F**). Considering ITGβ4 is expressed primarily in healthy airway epithelium and less diseased lungs (23), the loss of airway ITGβ4 expression with persistent airway remodeling suggests failed epithelial repair in DA-exposed rats.

Reduced airway ITGβ4+ expression associated with dysplastic airway remodeling and expansion of pan-cytokeratin+ cells in DA-exposed rats

To associate changes in airway *ITGβ4* protein expression with different airway epithelial cell types after DA exposure, co-staining was performed for ITGβ4 with the common club cell marker cytochrome p450 2F2 (Cyp2F2) (**Figure 2A**) or the ciliated cell marker acetylated alpha-tubulin (α-tubulin) (**Figure 2B**). Histologic evaluation was focused on the proximal, intrapulmonary airways (~250 μm) as these larger airways are the primary site of bronchial fibrosis in DA-exposed rats. In air-exposed airways, a small portion of Cyp2F2+ cells co-stained for ITGβ4+, however, most ITGβ4+ cells were both Cyp2F2- and α-tubulin-. Immediately following DA exposure, the airway epithelium appeared dysplastic with reduced Cyp2F2 staining and ITGβ4+ cells did not co-stain for Cyp2F2 nor α-tubulin. At 2 weeks, the airway epithelium appeared hyperplastic with staining for α-tubulin and Cyp2F2 primarily along the apical lumen. In contrast, ITGβ4 staining was below the airway epithelial luminal surface and without clear association to the basement membrane. By 5 weeks, airway Cyp2F2 and α-tubulin staining was comparable to air-exposed controls, but ITGβ4 airway expression remained reduced.

To begin to explore alternative markers in the dysplastic airway epithelium after DA exposure, immunofluorescent staining was performed for pan-cytokeratin (pan-CK) (**Figure 2C**). In air-exposed lungs, proximal airways were faintly pan-CK+ and linearly organized along the epithelium. Immediately following exposure, dysplastic airways stained intensely for pan-CK+. At 2 weeks, pan-CK+ cells persisted throughout the hyperplastic airway epithelium. By 5 weeks, pan-CK+ cells remained in the remodeled

airway epithelium but with reduced intensity. Collectively, the intrapulmonary airway epithelium of rats exposed to DA vapors demonstrate dysplastic remodeling with the progressive loss of ITGβ4+ cells and expansion of pan-CK+ cells but independent of Cyp2F2 and α-tubulin staining.

Primary human airway epithelial cells grown in 3D organoid cultures develop apoptosis with reduced ITGβ4 expression after DA exposure

To assess for ITGβ4 expression in human airway epithelial cells, primary airway epithelial cells were procured from deceased, human donor lungs and cultured in 3D organoid cultures (24, 25, 26) (**Figure 3, Supplemental Figures S2&S3**). Following 7 days in culture, organoids were exposed to DA and assessed for changes in number and diameter of organoids 3 days after exposure. First, brightfield microscopy and live/dead staining were performed in organoid cultures to assess organoid shape and cytotoxicity, respectively. With DA exposures, organoids lost their spherical shape with multiple cells dying along the apical surface of the organoids (**Figure 3A**). With DA exposure, the number of organoids per well did not differ between groups, however, organoid diameter decreased significantly in DA-exposed cultures vs. control cultures (**Figure 3B**). With caspase inhibition, the number of dead cells decreased in DA+ZVAD-FMK vs. DA alone (**Supplemental Figure S2**). Cell viability in DA-exposed organoids did not differ in percent surface area between young (D172) and adult donor (D403), suggestive that both adult and pediatric donors behaved similarly for their response to DA exposures. Considering the rho kinase inhibitor Y-27632 was added to cultures to maintain proliferation and may affect anoikis (27), cell viability was also assessed in the organoids

in the presence or absence of Y-27632 (**Supplemental Figure S3**). Cell viability after DA exposure did not differ with or without Y-27632. Hence, human airway epithelial organoids exposed to DA demonstrate reduced organoid diameter with increased airway epithelial cell death, primarily in apically-oriented airway epithelial cells.

Next, organoid cultures were assessed for common basal cell markers (28) - keratin 5 (Krt5), transcription factor delta N p63 (ΔNp63), and integrin beta 4 (ITGβ4) via immunocytochemistry (**Figure 3C**) and western blot (**Figure 3D**). In a subset of cultures, keratin 4 (Krt4) – a common marker of airway epithelial hillock and/or squamous cells (29) – was also assessed (**Supplemental Figure S4**). In control organoids, most cells stained positive for both Krt5 and ΔNp63 (**Figure 3C**), suggestive of a basal cell phenotype. Cells expressing ITGβ4 were located along the apical surface adjacent to the Matrigel substrate, while Krt4+ cells were primarily located away from the organoid's apical surface. With DA exposure, protein expression of ITGβ4 and ΔNp63 decreased while Krt5 expression did not differ between groups (**Figure 3D**)**.** Staining for Krt4 persisted in DA-exposed cultures. Hence, DA exposure in primary human airway organoid cultures reduced protein expression of the two canonical basal cell markers ΔNp63 and ITGβ4.

Diacetyl (DA) exposure induces adhesion-related apoptosis ('anoikis') in airway epithelial cells

To further delineate the mechanisms contributory to increased DA-induced epithelial cell death, human bronchial epithelial cells (16HBE14o-'s) were exposed to DA and monitored for viability up to 3 days after exposure. In DA-exposed cultures, cell confluence progressively decreased with respect to time (**Figure 4A**). In parallel, cleaved caspase

3/7 activity increased at Days 1 and 3 in DA-exposed cultures versus controls (**Figure 4B**), supportive of increased apoptosis. Cell viability was also assessed using immunocytochemistry staining after DA exposure (**Figure 4C**). Live cell surface area decreased while dead cell surface area increased in DA-exposed cultures compared to control cultures (**Figure 4D**). Collectively, DA-exposed airway epithelial cells demonstrate decreased live cell density and increased apoptosis days after exposure, suggestive of adhesion-related cell death or 'anoikis'.

DA-induced anoikis is partially mediated through caspase-mediated cleavage of integrin beta 4 (ITGβ4)

One proposed mechanism of DA-induced anoikis is through cleavage of integrin beta 4 (ITGβ4)(30). Integrin beta 4 (ITGβ4) is a large (202 kDa) protein with both an intracytoplasmic body and external cellular tail that connect airway epithelial cells to the adjacent basement membrane. The intracytoplasmic domain of ITGβ4 contains a caspase-mediated cleavage site near the C-terminus(31) (**Figure 5A**). Hence, DA-exposed cells were evaluated for total expression and cleavage byproducts of ITGβ4 via western blot as a potential mechanism of DA-induced anoikis. Total expression of ITGβ4 decreased while expression of lower molecular weight bands at previously identified molecular weights (79 and 130 kDa) affiliated with caspase-mediated cleavage sites(31) increased in DA-exposed cells compared to controls (**Figure 5B**). Hence, DA exposure induced cleavage of integrin beta 4 with the formation of lower molecular weight byproducts.

Next, the spatial distribution of ITGβ4 was assessed using immunocytochemistry staining of exposed airway epithelium (**Figure 5C & 5D**). In control cells, ITGβ4 expression was

located along the cytoplasmic membrane extending out towards the basement membrane (**Figure 5C & 5D**). With DA exposure, surface expression of ITGβ4 was reduced with perinuclear aggregation. When DA-exposed cells were co-treated with the caspase inhibitor ZVAD-FMK, surface expression of ITGβ4 was partially preserved with reduced aggregation of intracytoplasmic ITGβ4 compared to DA-exposed alone (**Figure 5D**).

Considering treatment with the pan-caspase inhibitor ZVAD-FMK reduced anoikis, we next assessed whether overexpression of ITGB4 via plasmid transfection could also promote ITGβ4 cytoplasmic localization. In cells not exposed to DA, overexpression of ITGB4 enhanced the cytoplasmic expression of ITGβ4 compared to control + empty plasmid alone (**Figure 5D** *bottom row*). In DA-exposed cultures, perinuclear aggregation of ITGβ4 occurred independent of treatment with ITGB4 or empty plasmid. In summary, DA exposure induced caspase-mediated cleavage of ITGβ4 with cellular re-distribution from the cytoplasm membrane to perinuclear aggregation. With caspase inhibition, cytoplasmic surface expression of ITGβ4 was partially preserved following DA exposure. Additionally, ITGB4 overexpression alone was insufficient to prevent DA-induced nuclear aggregation of ITGβ4, supporting a post-translational mechanism contributory to the cell's recovery after DA exposure.

Caspase inhibition prevents anoikis and partially promotes airway epithelial recovery

Considering that caspase inhibition improved ITGβ4 surface expression, airway epithelial cell cultures were next assessed for cell confluence, apoptosis and epithelial recovery after DA exposure. By brightfield imaging, the number of non-adherent cells decreased in DA-exposed treated with caspase inhibitor compared DA alone cultures (**Figure 6A**).

Dead staining also decreased in DA+ZVAD-FMK cultures compared DA alone (**Figure 6B**). Three additional viability assays were also performed (LDH, WST-1 and MTT) to verify reduced toxicity in DA+ZVAD-FMK (**Supplemental Figure S5**). In all three assays, cell viability improved in DA+ZVAD-FMK treated cells versus DA-exposed cells. Additionally, in both control and DA-exposed cells, supernatant cleaved caspase-3/7 activity was significantly reduced in ZVAD-FMK cultures compared to non-treated cultures (**Figure 6C**), supportive of reduced apoptosis.

ITGB4 transfection in airway epithelial cells improves gene expression but fails to prevent anoikis nor increase full length protein expression following DA exposure

Similar viability assays were performed in both non-exposed and DA-exposed cultures treated with empty vector or ITGB4 transfection. In DA-exposed cells transfected with ITGB4, the number of live cells increased in culture with improved cell confluence by both brightfield imaging and calcein AM staining compared to DA + empty plasmid transfection (**Figure 6A & 6B**). However, ITGB4 transfection failed to reduce the number of dead cells by staining nor by supernatant cleaved caspase-3/7 activity (**Figure 6B & 6C**).

To verify effective transfection of ITGB4, cells were collected and assessed for both RNA and protein expression. ITGB4 transfection was successful in overexpressing ITGB4 at the gene level as verified by RT-PCR (**Figure 7A**). In contrast, DA-exposed cells transfected with ITGB4 failed to show differ in protein expression relative to DA + plasmid (**Figure 7B & 7C**). With DA exposure, lower molecular weight bands persisted in DA + ITGB4 transfected cells, suggestive of persistent ITGβ4 cleavage.

To begin to explain the inefficient conversion from transcription to translation in DA-exposed, proteins associated with the integrated stress response (ISR) including C/EBP homologous protein (CHOP), eukaryotic initiation factor 2 alpha (eIF2α) and growth arrest and DNA damage-inducible protein (GADD34) were assessed in airway epithelial cells (**Figure 7D & 7E**). ISR activation is known to suppress protein translation following sustained ER stress, and with sustained stress, activate apoptosis (32). In DA-exposed cells, p-eIF2α and GADD34 protein expression increased compared to control via western blot, supportive of ISR activation (**Figure 7D**). By immunofluorescence, DA exposure promoted nuclear CHOP expression and not seen in control cultures (**Figure 7E**). Thus, one explanation for the ineffective translation of ITGβ4 despite increased ITGB4 transcription is the persistent activation of the ISR in DA-exposed cultures, impairing translational efficiency in those cells transcriptionally active for ITGB4 with downstream activation of CHOP. Collectively, caspase inhibition prevented DA-induced anoikis while ITGB4 overexpression via plasmid transfection failed to rescue DA-exposed airway epithelial cells with sustained ISR activation.

Discussion

Bronchiolitis obliterans (BO) is a common, end-stage histopathologic diagnosis that results from multiple different insults (5, 33). Airway epithelial injury is common to nearly all forms of BO. Here, rats exposed to occupationally-relevant concentrations of diacetyl (DA) develop significant bronchial fibrosis with reduced airway ITGβ4 expression and persistent sub-epithelial airway remodeling weeks after the initial exposure supportive of abnormal repair. In parallel, airway epithelial cells exposed to DA develop anoikis with cleavage of integrin beta 4 (ITGβ4). Caspase inhibition reduced DA-induced anoikis and improved ITGβ4 surface expression while ITGβ4 overexpression failed to prevent ITGβ4 cleavage with sustained activation of the integrated stress response. Collectively, these novel findings highlight the relevance of ITGβ4 cleavage in DA-induced airway epithelial anoikis in the context of BO pathology.

Integrin beta 4 (ITGβ4) is a large transmembrane protein commonly used as a surface marker for identifying airway epithelial progenitor cells (26). Integrin alpha 6 (ITGα6) is the only binding partner for ITGβ4 (23). This integrin pair of α6β4 is one of two epithelial receptor pairs common to healthy airway epithelium (23, 34). The primary function of α6β4 is to connect healthy airway epithelial cells to the basement membrane through laminin 332 (18, 35, 36). With severe damage to the airway epithelium following DA exposure, caspase-mediated cleavage of ITGβ4 developed with reduced surface and total ITGβ4 expression. We propose this loss of ITGβ4 is a common sentinel event in scar tissue formation. In support of this hypothesis, ITGβ4 is found in multiple other epidermally-derived organs such as the skin, eyes, and gastrointestinal tract. Epidermolysis bullosa (EB) is an inherited, heterogeneous group of genetic dermatoses characterized by

mucocutaneous fragility and blister formation(37, 38). Multiple genetic variants of ITGβ4 have been identified in junctional EB. Genetic mutations of EB give rise to mechanical disruption of structural proteins that influence epithelial cell adhesion integrity. Airway fibrosis is an infrequently reported sequalae of trauma or following severe respiratory tract infection in EB patients (38). This genetic disease affiliated with dysfunctional ITGβ4 supports loss and/or abnormal expression of ITGβ4 in airway epithelial cells as an important event contributory to airway remodeling.

While the integrity of the airway epithelium is imperative to repair, airway regeneration is not possible without a supportive basement membrane. Airway basal cells produce some provisional extracellular matrix, however, most extracellular matrix production originates from fibroblasts (39, 40). Human lung fibroblasts isolated from patients with BOS demonstrate impaired capacity to support airway epithelial progenitor cells as measured by colony-forming efficiency compared to healthy control fibroblasts (41). Similarly, in rats exposed to DA via intratracheal instillation who develop BO lesions, tenascin C is significantly increased in fibrotic airways compared to control-exposed airways (9). Tenascin C is an important extracellular matrix protein that accumulates in both inflammatory (42, 43) and fibrotic lung diseases (44, 45, 46, 47). With repetitive or persistent airway epithelial injury, the persistent production of tenascin-C leads to abnormal airway remodeling in mice (48). Thus, the development of airway remodeling in bronchiolitis obliterans is multicellular, however, the abnormal connection between airway epithelial cells and the supportive basement membrane matrix contributes substantially to airway pathway.

Integrin beta 4 (ITGβ4) is important to other fibrotic lung diseases, specifically pulmonary or 'parenchymal' fibrosis (49, 50, 51). Pulmonary fibrosis is a devastating disease of lung scarring in the distal lung parenchyma. In preclinical models of pulmonary fibrosis following severe influenza A viral (IAV; H1N1) respiratory infection, epithelial cells positive for Krt5 and ITGβ4 migrate and proliferate in the distal lung parenchyma concurrent with the development of lung fibrosis (50). The proliferation of these Krt5+ITGβ4+ 'pods' at sites of parenchymal fibrosis is considered pathologic (49), and an important histopathologic finding suggestive that other resident lung epithelial progenitor cell populations, such as the type II pneumocytes, failed in their reparative capacity. Pulmonary fibrosis is regionally distinct from that of BO, primarily affecting the lung parenchyma (5, 52). Hence, the model of influenza-induced lung fibrosis is different in the lung's compartment from the current model using DA. More specifically, DA reacts primarily with the proximal airway epithelium and less distal lung parenchyma due to its inherent reactive properties (53, 54). Here, we have identified reduced expression of airway ITGβ4 and persistent sub-epithelial remodeling weeks after DA exposures. These compartmental differences highlight important variation in preclinical models of lung fibrosis with the inverse expression changes of ITGβ4 relative to fibrotic disease.

In humans, airway basal cells are the primary progenitor cell of the proximal, intrapulmonary airway epithelium best characterized by dual positivity for Krt5 and delta N p63 (ΔNp63+) (26, 55). Following most inhalation exposures, epithelial repair occurs through migration, proliferation, and differentiation of airway basal cells (11, 56). Conversely, when challenged with certain environmental toxicants, significant damage occurs not only to the airway epithelium but to this rare population of airway epithelial

progenitor cells (57, 58). Other preclinical models of BO support this similar hypothesis (52). Specifically, the number of Krt5+ΔNp63+ airway basal cells is significantly reduced in ferrets who underwent orthotopic lung transplant and who subsequently develop BO. Similarly, the number of Krt5+ΔNp63+ basal cells isolated from human airways after lung transplant is inversely associated with bronchiolitis obliterans syndrome (BOS) (52). Likewise, the number of airway basal cells is significantly reduced in the trachea of mice exposed to high dose chlorine inhalation, a highly reactive chemical warfare agent associated with severe airway remodeling (57). These preclinical models highlight the relevance of airway basal cell injury and abnormal repair in BO. Future studies remain underway evaluating the role of ITGβ4 specifically in airway basal cell number and function as well as their association with DA-induced BO.

The current study is not without limitation. First, *in vitro* exposures occurred in submerged cultures rather than air-liquid interface (ALI) cultures to limit the heterogeneity of the airway cultures. ALI cultures consist of both ciliated and secretory cells in addition to airway basal cells. Future experiments using ALI cultures and pure DA vapor exposures will enhance the translational relevance of findings with isolation of basal cells. Second, primary human airway epithelial cells were obtained from deceased pediatric and adult lung donors. While no significant difference in DA-induced anoikis was seen between these two donors, these studies were not powered for certain biologic variables, including age, in our organoid exposure cultures. Third, the pan-caspase inhibitor was used to block ITGβ4 cleavage. Future studies are needed to delineate the specific caspases and associated sites on ITGβ4 modified after DA exposure. Last, neither caspase inhibition nor ITGβ4 overexpression were used in our *in vivo* rat model considering neither therapy

alone completely improved airway epithelial repair *in vitro*. Future studies targeting post-translational modifications and/or ISR activation are likely needed to significantly promote airway repair after DA exposures.

In summary, the current study significantly advances our understanding of DA-induced airway epithelial cell anoikis through caspase-mediated cleavage of ITGβ4. Identifying caspase-mediated cleavage of ITGβ4 after DA exposures is a sentinel event in failed airway epithelial repair and fibrotic airway remodeling. Future therapies targeting improved airway epithelial ITGβ4 expression may promote proper epithelial repair to prevent the devastating fibrotic airways disease BO currently with no FDA-approved medications.

Material & Methods

Chemicals

Diacetyl (DA; 2,3-butanedione) was purchased from Sigma-Aldrich (CAS no. 431-03-8, 99% pure; St. Louis, MO). Z-VAD-FMK was obtained from MCE (CAS no. 161401-82-7; Monmouth Junction, NJ). Dispase II powder was purchased from Gibco (catalog # 17105041; Grand Island, NY). Matrigel basement membrane matrix was acquired from Corning (catalog # 354234; Corning, NY). Lipofectamine 3000 was obtained from Invitrogen (catalog # L3000001; Carlsbad, CA)

Animals

All studies followed Institutional Animal Care and Use Committee (IACUC) guidelines and were approved by the University Committee on Animal Resources at the University of Rochester, Rochester, NY. Six to eight-week-old male Sprague-Dawley rats (Charles River Laboratory; Wilmington, WA, USA) weighing between 200-300 g were maintained in an AALAC accredited facility.

Primary Human Lung Epithelial Cells Grown in Ex Vivo Organoid Cultures

Two vials of whole lung digested, mixed lung cells, dissociated from a two-year-old male (Donor D172) or 49-year-old female (Donor 403) Transplant Network donor with no known lung disease were obtained from the LungMAP BRINDL repository. Initial studies were conducted using donor D172 with additional studies to assess for differences in airway epithelial response with respect to age. For passage 0 and 1, cells were cultured on a T75 flask in BEGM medium supplemented with 78 µg/ml bovine pituitary extract, 1.5 µg/ml bovine serum albumin fraction V 7.5%, 50 ng/ml retinol all-trans, 250 ng/ml

amphotericin B, 80 µg/ml gentamicin, 20 ng/ml epidermal growth factor as well as fibroblast inhibition cocktail containing 1 µmol dorsomorphin homolog 1 (DMH-1), 1 µmol activin receptor-like kinase (ALK), 10 µmol rho kinase inhibitor Y-27632, and 1 µmol glycogen synthase kinase 3 (GSK-3; 'CHIR')(24). After reaching 80% confluence, cells were dissociated from the flask, spun down and then suspended in airway medium (3:1 v/v F12 Nutrient Mixture and Dulbecco's Modified Eagle's Medium (DMEM)) supplemented with 5% fetal bovine serum, 9.4 µg/ml hydrocortisone, 5 µg/ml insulin, 8.4 ng/ml cholera toxin, 10 ng/ml epidermal growth factor, 24 µg/ml adenine, and 5 µmol Y-27632. The cells were mixed with chilled Matrigel (1:2) and seeded onto a 6-well culture plate with 2ml airway media.

Human Bronchial Epithelial Cell Line (16HBE14o-)

The human bronchial epithelial cell line (16HBE14o-, Millipore; Burlington, MA) was cultured in Minimum Essential Medium Eagle (α-MEM, Sigma; St. Louis, MO) supplemented with 10% fetal bovine serum (FBS; Corning, NY), 2 mM L-glutamine, and 1× penicillin–streptomycin solution (Thermo Fisher Scientific; Waltham, MA). Prior to cell culture, all flasks or plates were coated overnight with 34.5 µg/ml collagen I (Corning, NY) in 70% ethanol. All exposures were performed on cells at passage numbers <7. Authentication of the cells, including verification of common airway epithelial genes, was performed prior to any DA exposure.

In Vivo Diacetyl (DA) Exposures

In vivo DA vapor exposures were performed at the University of Rochester Medical Center (URMC) Inhalation Exposure Facility (IEF), as described previously (10, 21, 22).

In brief, whole body inhalation chambers were used for all exposures. Rats were placed inside single occupancy compartments of stainless-steel cages (8 rats / cage). Cages were then placed in Plexiglas exposure chambers within a ventilated fume hood. Animals were exposed to 200 parts-per-million (ppm) DA or filtered room air (RA) for 6 hours per day for five consecutive days. DA concentrations, temperature (24-28°C), and humidity (30-60%) were continuously monitored over the course of the exposures. Animal weights were performed prior to and three times weekly as outlined for 2 or 5 weeks post-exposure (*Schematic Figure 1*). Multiple DA exposures were performed for exposure replicates with representative datasets included for publication.

Lung tissue harvest, immunohistochemistry and immunofluorescent staining

Animals were euthanized with an intraperitoneal injection of Euthasol (pentobarbital sodium and phenytoin sodium, Vibrac, France) followed by aortic dissection. The right main bronchus was tied off and right lungs excised. The right lung lobes were immediately frozen (-80°C) for future analyses. The left lung was inflated and fixed in 10% neutral buffered formalin, desalted and dehydrated to 70% ethanol the following day. Lung tissue was then embedded, sectioned (5µm) and stained for hematoxylin and eosin (H&E).

Certain embedded lung sections were stained for integrin beta 4 (ITGβ4; CD104; 1:250, Abcam; Cambridge, MA, US; Cat. #ab29042), cytochrome p450 2F2 (Cyp2F2; 1:100, Santa Cruz, Dallas, TX, US; Cat # sc-374540), acetylated tubulin (α-tubulin; 1:500, Millipore Sigma, Burlington, MA, US; Cat# T7451), pan-cytokeratin (pan-CK; 1:100, Abcam, Cambridge, MA; Cat# ab7753), or rabbit IgG (1:200, Agilent; Santa Clara, CA, USA; negative control). Briefly, sections were deparaffinized with xylene and rehydrated with graded ethanol. Heat-mediated antigen retrieval was performed at 95°C for 20 minutes (Agilent; Santa Clara, CA, USA; Cat. #S236784). Slides were blocked for 30 min with 10% fetal bovine serum (FBS; Corning). Primary antibody was then applied overnight at 4°C. Following multiple washes, slides were incubated with a fluorescent secondary antibody (1:500, Invitrogen; Waltham, MA) for 1 hour, washed again and then mounted with DAPI Fluoromount medium (Southern Biotech; Birmingham, AL). Images were acquired using a fluorescence microscope (Leica DM6000; Wetzlar, Germany).

Hydroxyproline Assay

Following the manufacturer's protocol (Cayman Chemical, Ann Arbor, MI; Cat. #702440), 50 mg of rat lung tissue was homogenized in 500 µl of water, then hydrolyzed with 10 N NaOH. Samples were subsequently neutralized with 10 N HCl, oxidized and developed using the Hydroxyproline Assay Reagent in a stepwise manner. Absorbance was measured at 560 nm using a SpectraMax M5 microplate reader (Molecular Devices; San Jose, CA).

Western Blotting

Airway epithelial cells or rat lung tissue were homogenized in RIPA lysis buffer (Thermo Scientific; Rockford, IL) supplemented with a protease inhibitor cocktail (Roche; Mannheim, Germany). Following centrifugation at 12,000 rpm for 20 minutes at 4°C, soluble supernatant fractions were assessed for total protein and subsequent western blot. Total protein concentrations were determined using a BCA assay kit (Thermo Scientific; Rockford, IL). Ten micrograms (µg) of total protein were resolved in stain-free, pre-cast 4–15% gradient Tris–Glycine gels (Bio-Rad; Hercules, CA), then transferred to 0.2 µm nitrocellulose membranes (Pall Corporation, NY). The membrane was stained with primary antibodies for keratin 5 (KRT5; 1:2000, Biolegend; San Diego, CA; Cat. # Poly19055), integrin beta 4 (ITGβ4, CD104; 1:1000, Invitrogen; Waltham, MA; Cat. # PA5-17172), eukaryotic initiation factor 2 alpha (eIF2α, Cell Signaling #9722, 1:1000), p-eIF2α (Cell Signaling #9721, 1:1000), and delta N isoform of transcription factor p63 (ΔNp63; 1:1000, MilliporeSigma; Burlington, MA; Cat. #ABS552). HRP and SuperSignal West Pico chemiluminescent substrates (Thermo Scientific; Rockford, IL) were used to detect protein signal intensity. Image Lab software (Bio-Rad; Hercules, CA) was used for target protein normalization and quantification.

In Vitro Diacetyl (DA) Exposures

Once airway epithelial cell cultures reached >80% confluence, cells were exposed to DA (8.6 mM) by adding DA to the culture medium for one hour. DA concentrations were extrapolated from previous *in vitro* exposure experiments (11, 59, 60, 61). The approximate vapor-phase equivalent of the DA concentration is 387 ppm, based on previous extrapolated *in vitro* studies using a DA vapor cup exposure model (61). Following exposure, the cells were immediately rinsed with Dulbecco's phosphate-buffered saline (DPBS) and replenished with fresh epithelial cell medium or fresh medium supplemented with the pan-caspase inhibitor Z-VAD-FMK (20 µM). The concentration of Z-VAD-FMK was determined by LDH and caspase 3/7 activity assays as well as previously published literature using 16HBE14o- (62). Cells exposed to staurosporine (10 µM) for 4 hours were used as positive exposure controls for apoptosis. Following DA exposure, cultures were monitored for up to 3 consecutive days for recovery. All DA exposures were conducted in exposure replicates.

For primary cells grown in organoid cultures, DA exposures occurred 7 days after plating of dissociated cells in single cell suspensions. DA was added to the cultures submerged in airway media for 1 hour at the concentration specified above (8.6 mM). After exposure, similar monitoring occurred as described for 16HBE14o- cells above.

Plasmid Transfection

Using the manufacturer’s protocol (Invitrogen; Cat. # L3000001), lipofectamine 3000 reagent was diluted in FBS-free media. The purified pRK5 beta4 plasmid (ITGβ4; AddGene, Watertown, MA, USA; plasmid #16037) was added to the media followed by the P3000 reagent. The mixture was incubated for 20 minutes, after which the transfection

solution was added to the cells. After 4 hours of incubation at 37°C in 5% CO_2, FBS was added back to the culture.

Live/Dead Staining

Following standard protocol (ThermoFisher; Cat. #R37601), calcein AM (green, 'live') was mixed with BOBO-3 Iodide (deep red, 'dead'), and then equal volume added of the 2x stock to the cells in fresh media. Following 15 minutes at room temperature, the cells were imaged using a LEICA DM5500 B compound microscope with a LEICA DFC365 FX camera (Wetzlar, Germany).

Caspase-Glo 3/ 7 Assay

Following the standard Caspase-Glo 3/7 assay protocol (Promega Corp, Madison, WI; Cat. #G8091), buffered solution was mixed with the Caspase-Glo 3/7 substrate. Supernatants from experimental cells were added to a white-walled multi-well plate, followed by the addition of the reagent in equal volumes. The plate was incubated for 30 minutes at room temperature, and relative luminescence was measured using a SpectraMax M5 microplate reader (Molecular Devices; San Jose, CA).

Immunocytochemistry Staining

For 16HBE14o-'s, cells were grown on collagen-coated 15 mm coverslips (Chemglass Life Science; Vineland, NJ). On 3 days post-exposure, cells were fixed for 10 minutes using 4% paraformaldehyde (PFA) and then permeabilized with 0.1% Triton-X-100 in PBS for 15 minutes.

For both 16HBE14o-'s and organoids, fixed cells were blocked with 2% bovine serum albumin (BSA) in phosphate-buffered saline (PBS) for 1 hour and incubated overnight with the primary antibody against C/EBP homologous protein (CHOP; 1:250, Invitrogen #MA1-250), delta N isoform of transcription factor p63 (ΔNp63; 1:250, MilliporeSigma; Burlington, MA; Cat. #ABS552), integrin beta 4 (ITGβ4, CD104; 1:250, Abcam, Cambridge, MA; Cat # ab182120), Keratin 4 (Krt4; 1:500, Abcam, Cambridge, MA; Cat#ab51599), Keratin 5 (Krt5; 1:250, Invitrogen, Waltham, MA; Cat #MA5-12596), secretoglobin family 1A member 1 (scgb1a1; 1:500, Millipore Sigma, Burlington, MA, US; Cat # abs1673), or secretoglobin family 3A member 2 (scgb3a2; 1:500, R&D Systems, Minnepolis, MN, US; Cat # AF3465), or at 4°C. The cells were then washed; incubated

with a fluorescent secondary antibody (1:500, Invitrogen, Waltham, MA) for 1 hour; and mounted with DAPI Fluoromount medium (Southern Biotech, Birmingham, AL). Images were acquired using a fluorescence phase contrast microscope (Leica DM6000, Wetzlar, Germany), and relative expression change calculated relative to exposure controls via semi-quantitation using ImageJ (NIH, Bethesda, MD).

Immunohistochemistry

Airway epithelial organoids were cultured in chamber slides (Lab-Tek II, cat# 154534). Organoids were fixed in 10% neutral buffered formalin (NBF) for 24 hours at room temperature. A 2% low-melting point agarose solution was prepared in dH_2O, microwaved until dissolved, and allowed to cool to ~50°C. The agarose was then gently added dropwise to the organoids and allowed to polymerize for 30 minutes. The organoids, with the attached agarose, were excised using a surgical blade and secured into a tissue processing cassette with presoaked Kimwipes. The cassettes were stored in 10% neutral buffered formalin (NBF) for 24 hours and then transferred to 70% ethanol until processed into paraffin blocks and sectioned (5 µm) for immunohistochemistry as detailed above.

Statistics

Prior to any analysis, all data were graphed using Prism 9.0 (GraphPad; La Jolla, CA) assessing distribution and variance of each group. When data were normally distributed and with similar variance, a t-test (e.g. organoid numbers), an ordinary one-way ANOVA (e.g., DA exposure alone for multiple groups) or two-way ANOVA (exposure x treatment) was used with a p-value of 0.05. When standard deviation varied between groups, an unpaired t-test with Welch's correction or Welch's ANOVA test was performed. A Mann-Whitney test or Kruskal-Wallis test was performed on non-parametrically distributed populations. Only when a $p<0.05$ was identified as statistically significant by the primary analysis were post-hoc analyses performed with p-value adjusted for multiple comparisons using Dunnett's (parametric) or Dunn's (non-parametric). All exposures were run in replicates with at least 2 sample replicates per exposure group based on prior *in vivo*(10) and *in vitro*(11, 20, 59) exposures using DA. Randomization occurred for

group assignment prior to the initiation of exposure (e.g., DA vs. Air). For each exposure, 16 animals were exposed per group accounting for approximately 60% survival by 2 weeks post-exposure in the DA group. Investigators were blinded to exposure assignments.

References

1. Clark S, Winter CK. Diacetyl in Foods: A Review of Safety and Sensory Characteristics. Compr Rev Food Sci F. 2015;14(5):634-43.
2. Anders MW. Diacetyl and related flavorant alpha-Diketones: Biotransformation, cellular interactions, and respiratory-tract toxicity. Toxicology. 2017;388:21-9.
3. Akpinar-Elci M, Travis WD, Lynch DA, Kreiss K. Bronchiolitis obliterans syndrome in popcorn production plant workers. Eur Respir J. 2004;24(2):298-302.
4. Kreiss K, Gomaa A, Kullman G, Fedan K, Simoes EJ, Enright PL. Clinical bronchiolitis obliterans in workers at a microwave-popcorn plant. N Engl J Med. 2002;347(5):330-8.
5. Barker AF, Bergeron A, Rom WN, Hertz MI. Obliterative bronchiolitis. N Engl J Med. 2014;370(19):1820-8.
6. van Rooy FG, Rooyackers JM, Prokop M, Houba R, Smit LA, Heederik DJ. Bronchiolitis obliterans syndrome in chemical workers producing diacetyl for food flavorings. Am J Respir Crit Care Med. 2007;176(5):498-504.
7. Morgan DL, Merrick BA, Gerrish KE, Stockton PS, Wang Y, Foley JF, et al. Gene expression in obliterative bronchiolitis-like lesions in 2,3-pentanedione-exposed rats. PLoS One. 2015;10(2):e0118459.
8. Morgan DL, Jokinen MP, Price HC, Gwinn WM, Palmer SM, Flake GP. Bronchial and bronchiolar fibrosis in rats exposed to 2,3-pentanedione vapors: implications for bronchiolitis obliterans in humans. Toxicol Pathol. 2012;40(3):448-65.
9. Palmer SM, Flake GP, Kelly FL, Zhang HL, Nugent JL, Kirby PJ, et al. Severe airway epithelial injury, aberrant repair and bronchiolitis obliterans develops after diacetyl instillation in rats. PLoS One. 2011;6(3):e17644.
10. Wang J, Kim SY, House E, Olson HM, Johnston CJ, Chalupa D, et al. Repetitive diacetyl vapor exposure promotes ubiquitin proteasome stress and precedes bronchiolitis obliterans pathology. Arch Toxicol. 2021;95(7):2469-83.
11. McGraw MD, Kim SY, Reed C, Hernady E, Rahman I, Mariani TJ, et al. Airway basal cell injury after acute diacetyl (2,3-butanedione) vapor exposure. Toxicol Lett. 2020;325:25-33.
12. Hubbs AF, Fluharty KL, Edwards RJ, Barnabei JL, Grantham JT, Palmer SM, et al. Accumulation of Ubiquitin and Sequestosome-1 Implicate Protein Damage in Diacetyl-Induced Cytotoxicity. Am J Pathol. 2016;186(11):2887-908.
13. Hubbs AF, Goldsmith WT, Kashon ML, Frazer D, Mercer RR, Battelli LA, et al. Respiratory toxicologic pathology of inhaled diacetyl in sprague-dawley rats. Toxicol Pathol. 2008;36(2):330-44.

14. Hao D, Liu Y, Li L, Stripp BR, Chen H. Immunological and regenerative properties of lung stem cells. Physiol Rev. 2026;106(1):485-527.
15. Crystal RG, Randell SH, Engelhardt JF, Voynow J, Sunday ME. Airway epithelial cells: current concepts and challenges. Proc Am Thorac Soc. 2008;5(7):772-7.
16. Stem/Progenitor Cells and Lung Repair. Chairman Summary of the Twenty-Third Transatlantic Airway Conference. 2008. Proc Am Thorac Soc. 2008;5(6):672-4.
17. Flake GP, Morgan DL. Pathology of diacetyl and 2,3-pentanedione airway lesions in a rat model of obliterative bronchiolitis. Toxicology. 2017;388:40-7.
18. Walko G, Castanon MJ, Wiche G. Molecular architecture and function of the hemidesmosome. Cell Tissue Res. 2015;360(3):529-44.
19. de Pereda JM, Ortega E, Alonso-Garcia N, Gomez-Hernandez M, Sonnenberg A. Advances and perspectives of the architecture of hemidesmosomes: lessons from structural biology. Cell Adh Migr. 2009;3(4):361-4.
20. Kim SY, McGraw MD. Post-translational modifications to hemidesmosomes in human airway epithelial cells following diacetyl exposure. Sci Rep. 2022;12(1):9738.
21. House EL, Kim SY, Chalupa D, Hernady E, Groves AM, Johnston CJ, et al. IL-17A neutralization fails to attenuate airway remodeling and potentiates a proinflammatory lung microenvironment in diacetyl-exposed rats. Am J Physiol Lung Cell Mol Physiol. 2023;325(4):L434-L46.
22. House EL, Kim SY, Johnston CJ, Groves AM, Hernady E, Misra RS, et al. Diacetyl Vapor Inhalation Induces Mixed, Granulocytic Lung Inflammation with Increased CD4(+)CD25(+) T Cells in the Rat. Toxics. 2021;9(12).
23. Sheppard D. Functions of pulmonary epithelial integrins: from development to disease. Physiol Rev. 2003;83(3):673-86.
24. Wang Q, Bhattacharya S, Mereness JA, Anderson C, Lillis JA, Misra RS, et al. A novel in vitro model of primary human pediatric lung epithelial cells. Pediatr Res. 2020;87(3):511-7.
25. Rock JR, Gao X, Xue Y, Randell SH, Kong YY, Hogan BL. Notch-dependent differentiation of adult airway basal stem cells. Cell Stem Cell. 2011;8(6):639-48.
26. Rock JR, Onaitis MW, Rawlins EL, Lu Y, Clark CP, Xue Y, et al. Basal cells as stem cells of the mouse trachea and human airway epithelium. Proc Natl Acad Sci U S A. 2009;106(31):12771-5.
27. Schmelzle T, Mailleux AA, Overholtzer M, Carroll JS, Solimini NL, Lightcap ES, et al. Functional role and oncogene-regulated expression of the BH3-only factor Bmf in mammary epithelial anoikis and morphogenesis. Proc Natl Acad Sci U S A. 2007;104(10):3787-92.
28. Ghosh M, Helm KM, Smith RW, Giordanengo MS, Li B, Shen H, et al. A single cell functions as a tissue-specific stem cell and the in vitro niche-forming cell. Am J Respir Cell Mol Biol. 2011;45(3):459-69.
29. Lin B, Shah VS, Chernoff C, Sun J, Shipkovenska GG, Vinarsky V, et al. Airway hillocks are injury-resistant reservoirs of unique plastic stem cells. Nature. 2024;629(8013):869-77.
30. Carroll DK, Carroll JS, Leong CO, Cheng F, Brown M, Mills AA, et al. p63 regulates an adhesion programme and cell survival in epithelial cells. Nat Cell Biol. 2006;8(6):551-61.

31. Werner ME, Chen F, Moyano JV, Yehiely F, Jones JC, Cryns VL. Caspase proteolysis of the integrin beta4 subunit disrupts hemidesmosome assembly, promotes apoptosis, and inhibits cell migration. J Biol Chem. 2007;282(8):5560-9.
32. Pakos-Zebrucka K, Koryga I, Mnich K, Ljujic M, Samali A, Gorman AM. The integrated stress response. EMBO Rep. 2016;17(10):1374-95.
33. Moonnumakal SP, Fan LL. Bronchiolitis obliterans in children. Curr Opin Pediatr. 2008;20(3):272-8.
34. Eble JA, Wucherpfennig KW, Gauthier L, Dersch P, Krukonis E, Isberg RR, et al. Recombinant soluble human alpha 3 beta 1 integrin: purification, processing, regulation, and specific binding to laminin-5 and invasin in a mutually exclusive manner. Biochemistry. 1998;37(31):10945-55.
35. Seltmann K, Cheng F, Wiche G, Eriksson JE, Magin TM. Keratins Stabilize Hemidesmosomes through Regulation of beta 4-Integrin Turnover. Journal of Investigative Dermatology. 2015;135(6):1609-20.
36. de Pereda JM, Lillo MP, Sonnenberg A. Structural basis of the interaction between integrin alpha6beta4 and plectin at the hemidesmosomes. EMBO J. 2009;28(8):1180-90.
37. Stublar A, Dragos V, Dolenc-Voljc M. Inherited epidermolysis bullosa: epidemiology and patient care in Slovenia with a review of the updated classification. Acta Dermatovenerol Alp Pannonica Adriat. 2021;30(2):63-6.
38. Bardhan A, Bruckner-Tuderman L, Chapple ILC, Fine JD, Harper N, Has C, et al. Epidermolysis bullosa. Nat Rev Dis Primers. 2020;6(1):78.
39. Coraux C, Roux J, Jolly T, Birembaut P. Epithelial cell-extracellular matrix interactions and stem cells in airway epithelial regeneration. Proc Am Thorac Soc. 2008;5(6):689-94.
40. White ES. Lung extracellular matrix and fibroblast function. Ann Am Thorac Soc. 2015;12 Suppl 1(Suppl 1):S30-3.
41. Zhang SB, Sun X, Wu Q, Wu JP, Chen HY. Impaired Capacity of Fibroblasts to Support Airway Epithelial Progenitors in Bronchiolitis Obliterans Syndrome. Chin Med J (Engl). 2016;129(17):2040-4.
42. Yasuda M, Harada N, Harada S, Ishimori A, Katsura Y, Itoigawa Y, et al. Characterization of tenascin-C as a novel biomarker for asthma: utility of tenascin-C in combination with periostin or immunoglobulin E. Allergy Asthma Clin Immunol. 2018;14:72.
43. Karjalainen EM, Lindqvist A, Laitinen LA, Kava T, Altraja A, Halme M, et al. Airway inflammation and basement membrane tenascin in newly diagnosed atopic and nonatopic asthma. Respir Med. 2003;97(9):1045-51.
44. Brissett M, Veraldi KL, Pilewski JM, Medsger TA, Jr., Feghali-Bostwick CA. Localized expression of tenascin in systemic sclerosis-associated pulmonary fibrosis and its regulation by insulin-like growth factor binding protein 3. Arthritis Rheum. 2012;64(1):272-80.
45. Carey WA, Taylor GD, Dean WB, Bristow JD. Tenascin-C deficiency attenuates TGF-ss-mediated fibrosis following murine lung injury. Am J Physiol Lung Cell Mol Physiol. 2010;299(6):L785-93.
46. Kuhn C, Mason RJ. Immunolocalization of SPARC, tenascin, and thrombospondin in pulmonary fibrosis. Am J Pathol. 1995;147(6):1759-69.

47. Paivaniemi O, Alho H, Maasilta P, Vainikka T, Salminen US. Tenascin is expressed in post-transplant obliterative bronchiolitis. Transplant Proc. 2006;38(8):2694-6.
48. Snyder JC, Zemke AC, Stripp BR. Reparative capacity of airway epithelium impacts deposition and remodeling of extracellular matrix. Am J Respir Cell Mol Biol. 2009;40(6):633-42.
49. Kanegai CM, Xi Y, Donne ML, Gotts JE, Driver IH, Amidzic G, et al. Persistent Pathology in Influenza-Infected Mouse Lungs. Am J Respir Cell Mol Biol. 2016;55(4):613-5.
50. Vaughan AE, Brumwell AN, Xi Y, Gotts JE, Brownfield DG, Treutlein B, et al. Lineage-negative progenitors mobilize to regenerate lung epithelium after major injury. Nature. 2015;517(7536):621-5.
51. Chapman HA, Li X, Alexander JP, Brumwell A, Lorizio W, Tan K, et al. Integrin alpha6beta4 identifies an adult distal lung epithelial population with regenerative potential in mice. J Clin Invest. 2011;121(7):2855-62.
52. Swatek AM, Lynch TJ, Crooke AK, Anderson PJ, Tyler SR, Brooks L, et al. Depletion of Airway Submucosal Glands and TP63(+)KRT5(+) Basal Cells in Obliterative Bronchiolitis. Am J Respir Crit Care Med. 2018;197(8):1045-57.
53. Zaccone EJ, Goldsmith WT, Shimko MJ, Wells JR, Schwegler-Berry D, Willard PA, et al. Diacetyl and 2,3-pentanedione exposure of human cultured airway epithelial cells: Ion transport effects and metabolism of butter flavoring agents. Toxicol Appl Pharmacol. 2015;289(3):542-9.
54. Fedan JS, Dowdy JA, Fedan KB, Hubbs AF. Popcorn worker's lung: in vitro exposure to diacetyl, an ingredient in microwave popcorn butter flavoring, increases reactivity to methacholine. Toxicol Appl Pharmacol. 2006;215(1):17-22.
55. Rock JR, Randell SH, Hogan BL. Airway basal stem cells: a perspective on their roles in epithelial homeostasis and remodeling. Dis Model Mech. 2010;3(9-10):545-56.
56. Chu CY, Kim SY, Pryhuber GS, Mariani TJ, McGraw MD. Single-cell resolution of human airway epithelial cells exposed to bronchiolitis obliterans-associated chemicals. Am J Physiol Lung Cell Mol Physiol. 2024;326(2):L135-L48.
57. O'Koren EG, Hogan BL, Gunn MD. Loss of basal cells precedes bronchiolitis obliterans-like pathological changes in a murine model of chlorine gas inhalation. Am J Respir Cell Mol Biol. 2013;49(5):788-97.
58. McGraw MD, Dysart MM, Hendry-Hofer TB, Houin PR, Rioux JS, Garlick RB, et al. Bronchiolitis Obliterans and Pulmonary Fibrosis after Sulfur Mustard Inhalation in Rats. Am J Resp Cell Mol. 2018;58(6):696-705.
59. Foster MW, Gwinn WM, Kelly FL, Brass DM, Valente AM, Moseley MA, et al. Proteomic Analysis of Primary Human Airway Epithelial Cells Exposed to the Respiratory Toxicant Diacetyl. J Proteome Res. 2017;16(2):538-49.
60. Brass DM, Gwinn WM, Valente AM, Kelly FL, Brinkley CD, Nagler AE, et al. The Diacetyl-Exposed Human Airway Epithelial Secretome: New Insights into Flavoring-Induced Airways Disease. Am J Respir Cell Mol Biol. 2017;56(6):784-95.
61. Kelly FL, Sun J, Fischer BM, Voynow JA, Kummarapurugu AB, Zhang HL, et al. Diacetyl induces amphiregulin shedding in pulmonary epithelial cells and in experimental bronchiolitis obliterans. Am J Respir Cell Mol Biol. 2014;51(4):568-74.

62. Sourdeval M, Lemaire C, Deniaud A, Taysse L, Daulon S, Breton P, et al. Inhibition of caspase-dependent mitochondrial permeability transition protects airway epithelial cells against mustard-induced apoptosis. Apoptosis. 2006;11(9):1545-59.

Acknowledgements

Special thanks to Dr. Michael O'Reilly and Min Yee for providing antibodies specific to airway club cells. Additional thanks to the Wilmot Cancer Center Histology Core (Director: Dr. Brian Marples; technical assistance: Eric Hernady), the Inhalation Exposure Facility (Director: Dr. Alison Elder; technical assistance: David Chalupa, MS), and the Donor families and the Biorepository for INvestigation of Diseases of the Lung (BRINDL) at the University of Rochester Medical Center. Of note, Figure 1A was created in Biorender McGraw, M. (2025) with publication license https://BioRender.com/gy9o3ht.

Conflict of Interest Statement

There are no competing financial interests in relation to this original work.

Author Contribution Statement

Conception and design (SYK, MDM); data acquisition (SYK, AP, HH, MDM); analysis and interpretation (SYK, MDM, GSP, TJM); manuscript draft, revisions and approval (SYK, AP, HH, GSP, TJM, MDM).

Ethics Statement

All animal studies were approved by the Institutional Animal Care and Use Committee of the University of Rochester Medical Center (URMC). All methods adhered to the National Institutes of Health Guidelines. The University of Rochester Research Study Review Board has reviewed and approved a human subject exemption, considering all donors were deceased (RSRB00047606).

Funding Statement

Work supported by grants from NIH NIEHS P30-ES001247 (MDM) and NIEHS K08-ES033290 (MDM), NHLBI U01HL122700 and U01HL148861 (GSP).

Data Availability

Reserved DOI available on FigShare and will be made public at time of publication at: https://figshare.com/account/articles/28385522

Figure Legends

Figure 1. Rats exposed repetitively to diacetyl vapors develop severe airway remodeling with increased and reduced lung integrin beta 4 expression. *(A)* Exposure schema of Sprague-Dawley rats exposed to 200 parts-per-million diacetyl (DA) vapors for 6 hours daily over 5 consecutive days (yellow bar) and then monitored for up to 5 weeks post-exposure. *(B)* Representative images of hematoxylin & eosin (H&E – 2x *first row* and –10x *second row*) or Trichrome (10x *third row*) - stained lung sections from rats exposed to Room Air (*far left column*), Diacetyl - end of exposure (Day 5; *middle left*), Diacetyl – 2 weeks post-exposure (*middle right*), and Diacetyl – 5 weeks post-exposure (*far right*) (*scale bar: 2mm; black box associates specific rat airway imaged under higher magnification*). Representative intrapulmonary rat bronchus for each group (*scale bar: 500 µm*; '*A' denotes intrapulmonary airway lumen; 'v' denotes adjacent bronchial vessel)* *(C)* Rat lung collagen content (µg/ml) via hydroxyproline assay. Lung collagen content increased in DA–exposed rats at the end of exposure (Day 5; *red closed circles; 359.0 (206.7)*) versus rats exposed to Room Air (*blue closed circles; 40.2 (36.4)*), but did not differ in Diacetyl – exposed rats at 2 weeks post-exposure (*red open circles; 300.2 (228.0)*) nor Diacetyl – exposed at 5 weeks post-exposure (*right; red half circles; 112.6 (81.1)*) vs. Room Air (n=4/group; ANOVA with Dunnett's correction, * p=0.048). (*D*) Representative western blots of integrin beta 4 (ITGβ4; *202 kDa, top row*), pro-caspase-3 and cleaved-caspase-3 (*middle rows, 35 and 19 kDa, respectively*) and GAPDH (*control, bottom row, 36 kDa*) from rat lung homogenates in air-exposed (*left*), DA-exposed lungs harvested at end of exposure (*Day 5; middle left*), DA-exposed at 2 weeks post-exposure (*middle right*) and DA-exposed lungs at 5 weeks post-exposure (*right*) (n=

3-4 / group). (*E*) Higher magnification immunofluorescent images of ITGβ4 (*green*) with DAPI (*blue*) in Room Air-exposed (*left*) and Diacetyl-exposed (*right*) at 5 weeks (*scale bar: 50 μm*).

Figure 2. Diacetyl-exposed rat airways lose integrin beta 4 protein expression with the expansion of pan-cytokeratin positive airway epithelial cells independent of ciliated and club cell staining. (A) Proximal intrapulmonary rat airways sections co-stained for club cell marker cytochrome p450 2F2 (Cyp2F2; *red*), integrin beta 4 (ITGβ4; *green*), and DAPI (*blue*) and imaged at 20x (scale bar: 250 µm; *top row*). Exposure groups include air control (*top row*), DA Day 5 (*second row*), DA Day 19 (*third row*), and DA 5 weeks (*fourth row*). (*B*) Proximal intrapulmonary rat airways sections co-stained for ciliated cell marker acetylated alpha-tubulin (α-tubulin; *red*), integrin beta 4 (ITGβ4; *green*), and DAPI (*blue*) and imaged at 20x (scale bar: 250 µm; *top row*). (C) Proximal intrapulmonary rat airways sections stained for pan-cytokeratin (pan-CK; *red*) and DAPI (*blue*) and imaged at 20x (scale bar: 250 µm; *top row*).

Figure 3. Primary human airway epithelial cells grown *ex vivo* in 3D organoid culture and exposed to diacetyl develop reduced organoid diameter and reduced basal cell expression. *(A)* Representative airway epithelial organoids imaged using brightfield (*left column*) or immunofluorescence (*right column*) and stained for calcein AM ('live', *green*) and BOBO-3 Iodide deep red ('dead', *red*) in control cultures (*top row*) and DA-exposed cultures (*bottom*). (*scale bar: 100 µm*). *(B)* Number of organoids per 10,000 cells plated (*top*) and organoid diameter (*bottom*) in non-exposed cultures (*blue circles*) and DA-exposed cultures (*red circles*) enumerated at Day 3 post-exposure (n=3 exposures x 4 replicates/group). The number of organoids did not differ statistically between DA and controls (t-test , p=0.54; Control – 496.9 (163.5) vs. Diacetyl - 446.5 (234.1)), while organoid diameter was significantly reduced in DA-exposed vs. non-

exposed cultures (t-test, **p = 0.008; Control – 151.6 (68.9) vs. Diacetyl – 71.0 (67.3)). *(C)* Representative immunofluorescent images of control (*top row*) and DA exposed (*bottom row*) organoids (5 µm FFPE sections) stained for keratin 5 (*Krt5; left column, red*), delta N isoform of p63 *(ΔNp63; middle column, red*), and integrin beta 4 (*ITGβ4; right column, red*) counterstained for DAPI (*blue*) (*scale bar: 50 µm*). *(D)* Representative western blots for Krt5, ΔNp63, and ITGβ4 relative to loading control GAPDH in primary human airway epithelial cells grown in organoid cultures and harvested 3 days after control (*left 6 lanes*) versus DA-exposed cultures (*right 5 lanes*). Relative protein expression of Krt5, ΔNp63 and ITGβ4 relative to GAPDH in DA-exposed organoids (*red circles*) compared to control (*blue circles*). Krt5 protein expression was not statistically reduced (p=0.49; Control – 1.0 (0.2) vs. Diacetyl – 1.0 (0.1)) while ΔNp63 and ITGβ4 expressions were statistically reduced in DA-exposed vs. control cultures (**p=0.005; Control – 1.1 (0.1) vs. Diacetyl – 0.5 (0.2) and ****p<0.0001; Control – 1.2 (0.1) vs. Diacetyl – 0.6 (0.1), respectively; n = 5-6 / group; t-tests with Welch's correction).

Figure 4. Human airway epithelial cells exposed to diacetyl (DA) undergo adhesion-related apoptosis ('anoikis'). (*A*) Brightfield images obtained of human bronchial epithelial cells (16HBE14o) exposed to control (PBS; *top left*), diacetyl (DA) at Day 1 (*top right*), Day 2 (*bottom left*), and Day 3 (*bottom right*; scale bar: 200 µm). Cells exposed to DA show progressive loss of confluence with detachment of large sheets of cells by Day 3 post-exposure. (*B*) Supernatant cleaved caspase 3/7 activity from exposed 16HBE14o- in control at Day 1 (*solid blue;* 5.2 (0.5) x 10^4), control at Day 3 (*hollow blue;* 8.2 (0.5) x 10^4), DA at Day 1 (*solid red;* 11.8 (3.9) x 10^4), and DA at Day 3 (*hollow red;* 18.2 (4.0) x

10^4) expressed as relative luminescence units (n=6/group; ****p<0.0001, Welch's ANOVA with Dunnett's correction; Day 1 *p = 0.043 (0.4and Day 3 **p = 0.0087). (*C*) Representative fluorescent images of 16HBE14o- stained with calcein AM ('live', *green*) and BOBO-3 Iodide deep red ('dead', *red*) in control (*top*), DA (middle), and control treated with 10 µM staurosporine for 4 hours at Day 3 (scale bar: 200 µm). (*D*) Semi-quantification of percentage area of live or dead fluorescent images relative to control. Square black bar columns represent cultures treated with staurosporine (Live – 58.1 (4.7) and Dead – 41.7 (5.4)). (n=6/group; unpaired t-tests with Welch's correction, DA Live – 50.6 (7.9) vs Control Live – 99.8 (3.3), ****p<0.0001; DA Dead – 15.0 (4.1) vs. Control Dead – 1.1 (0.6), **p=0.0021).

Figure 5. Caspase-mediated cleavage of integrin beta 4 after diacetyl exposure. *(A)* Schematic diagram of integrin beta 4 (ITGβ4), a large transmembrane protein with an extracellular domain located on the N-terminus (*left*) and cytoplasmic domain located by the C-terminus (*right*). Proposed caspase 3/7 cleavage site located within the cytoplasmic domain approximately 79 kDa from the C-terminus. Following cleavage, a 130 kDa fragment, inclusive of the extracellular domain, is formed. *(B)* Representative western blot of ITGβ4 (*molecular weight 202 kDa*) expressed in 16HBE14o- and previously exposed to PBS (*control, left 2 lanes*) and diacetyl (DA; *right 2 lanes*) at Day 3 post-exposure. In DA-exposed cells, lower molecular weight bands develop at 130 kDa and 79 kDa. *(C)* Representative immunofluorescent images of 16HBE14o- cells stained for ITGβ4 (*red*) in exposed controls (*left*) or DA; *(right*) at Day 3 post-exposure. (*Scale bar: 200 µm; white arrow denotes intracytoplasmic distribution of ITGβ4 in DA-exposed cells that is not seen in control cells)*. *(D)* Representative immunofluorescent images of 16HBE14o- cells

stained for ITGβ4 (*red*) and DAPI (*blue*) in exposed controls (*left top*), control+plasmid (*left bottom*), control + ZVAD-FMK (*left middle top*), control + ITGβ4 transfection (*left middle bottom*), DA *(right middle top*), DA + plasmid (*right middle bottom),* and DA+ZVAD-FMK (*right top*), DA + + ITGβ4 transfection (*right bottom*) at Day 3 post-exposure (*scale bar: 10 μm).*

Figure 6. Caspase inhibition but not ITGB4 transfection in diacetyl-exposed cells prevents late-onset anoikis. *(A)* Brightfield images of human bronchial epithelial cells (16HBE14o-) exposed to control (*PBS; top row*), or diacetyl (*DA; bottom row*) and treated with caspase inhibitor (ZVAD-FMK; *second column*), empty plasmid (negative control; *third column*), or plasmid containing integrin beta 4 (ITGβ4; *final column*). Images were obtained at Day 3 post-exposure. DA-exposed cells show areas of reduced confluence. In DA+ZVAD-FMK, the extent of epithelial detachment is reduced, and cell confluence is improved. Diacetyl-exposed cells treated with ITGβ4 demonstrate improved cell confluence, but persistent epithelial detachment. *(B)* Representative immunocytochemistry images of 16HBE's stained with calcein AM (*green*) and BOBO-3 Iodide deep red (*red*) in control (*top row*) or DA (*bottom row*) and treated with caspase inhibitor (ZVAD-FMK, *middle 2nd column*), empty plasmid (negative control, *3rd column*), or plasmid containing ITGβ4 (*4th column*). Images obtained at Day 3 after exposure (*scale bar: 200 μm*). *(C)* Supernatant cleaved caspase 3/7 activity from 16HBE's exposed to PBS control (*blue*) or DA *(red*) and treated with ZVAD-FMK (*hollow circle*), empty plasmid (*hollow triangle*), or plasmid containing ITGβ4 (*hollow square*) (n=6/condition; Welch's two-way ANOVA with Dunnett's correction, ****p<0.0001). Supernatant cleaved caspase

3/7 activity is proportional to assay luminescence (*relative units*). Caspase activity was significantly reduced in control (14.5 (1.1) x 10^4) vs. control + ZVAD-FMK (0.06 (0.04) x 10^4) and DA (44.1 (4.4) x 10^4) vs. DA+ZVAD-FMK (0.1 (0.04) x 10^4) (****p<0.0001 for both).

Figure 7. ITGB4 transfection increases gene expression in diacetyl-exposed cells but failed to prevent caspase-mediated cleavage of ITGβ4. *(A)* Integrin beta 4 gene expression (ITGB4) gene expression for each exposure condition relative to PPIA (n=4/group, Welch's two-way ANOVA for exposure x treatment with Dunnett's correction, ****p<0.0001). ITGB4 gene expression was significantly increased in those cells exposed to DA and transfected (DA + ITGβ4 – 5.37 (6.14) x10^4 versus DA + empty plasmid transfection - 0.33 (0.26) (**p=0.0095). *(B)* Representative western blots of integrin beta 4 (ITGβ4; molecular weight 202 kDa, cleaved ITGβ4 at 130 kDa and 79 kDa) expressed in 16HBE14o- for each group (*rows left to right*): PBS (control), control + plasmid, control + pan-caspase inhibitor (ZVAD-FMK), control + ITGβ4 transfection, control + ZVAD-FMK + ITGβ4 transfection, diacetyl (DA), DA + plasmid, DA + ZVAD-FMK, DA + ITGβ4 transfection, and control + staurosporine (10 µM). β-actin provided as loading control. (*C*) Semi-quantitation of ITGβ4 western blot from Fig. 7B at designated molecular weights. DA exposure reduced ITGβ4 expression at 202kDa (DA – 0.10 (0.10) (*red circles*) vs. Control – 1.00 (0.04) (blue circles)) with increased expression at 130 kDa (DA - DA – 1.9 (0.2) vs. Control – 1.0 (0.3)) and at 79 kDa (DA – 6.4 (1.6) vs. Control – 1.00 (0.02) (n=3-4/group, 2-way ANOVA for exposure x treatment; exposure - ****p<0.0001). *(D)* Representative western blots of integrin beta 4 (ITGβ4; molecular weight 202 kDa),

phosphorylated (p) – EIF2 alpha (α) (36 kDa), total EIF2α (36 kDa), GADD34 (100 kDa), and loading control GAPDH (36 kDa) in human bronchial epithelial (16HBE) control cell homogenates (*left two columns*) and diacetyl-exposed cell homogenates (*right two columns*). (E) Representative immunofluorescent images of 16HBE cells stained for C/EBP homologous protein (CHOP; *red*) + DAPI (*blue*) (*top row*) and following exposure in control (*top*) or DA-exposed (*bottom*) at Day 3 post-exposure. (*scale bar: 200 μm*).

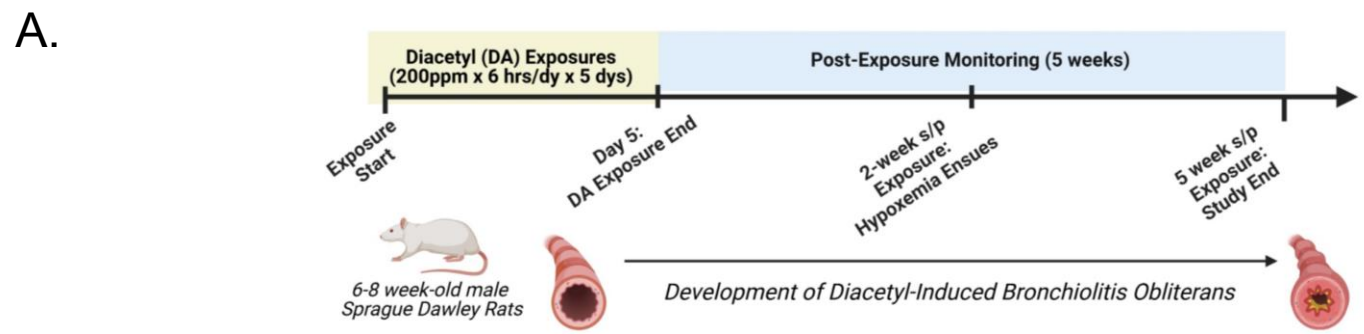
A.
Diacetyl (DA) Exposures
(200ppm x 6 hrs/dy x 5 dys)
Post-Exposure Monitoring (5 weeks)
Exposure Start
Day 5: DA Exposure End
2-week s/p Exposure: Hypoxemia Ensues
5 week s/p Exposure: Study End
6-8 week-old male Sprague Dawley Rats
Development of Diacetyl-Induced Bronchiolitis Obliterans

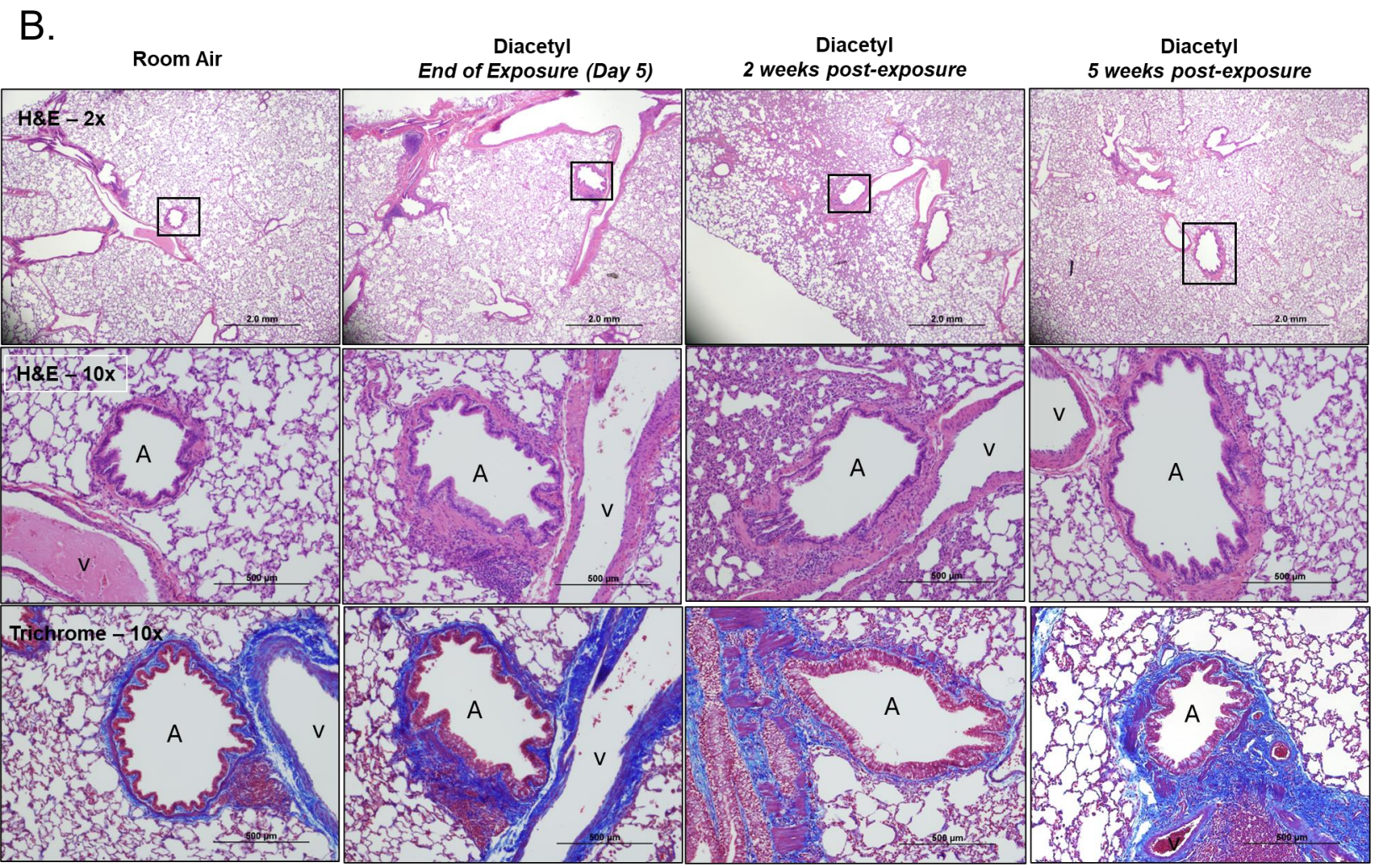
B.
Room Air
Diacetyl
End of Exposure (Day 5)
Diacetyl
2 weeks post-exposure
Diacetyl
5 weeks post-exposure
H&E – 2x
H&E – 10x
Trichrome – 10x
A
V
2.0 mm
500 µm

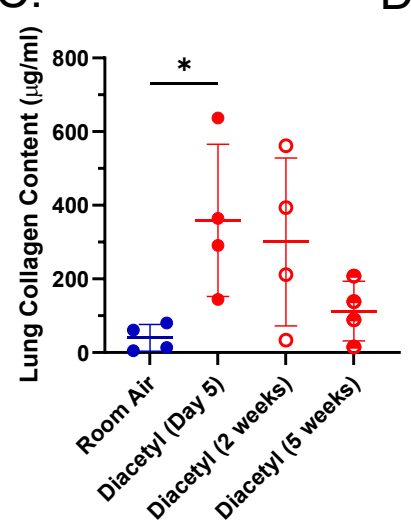
C.
Lung Collagen Content (µg/ml)
800
600
400
200
0
*
Room Air
Diacetyl (Day 5)
Diacetyl (2 weeks)
Diacetyl (5 weeks)

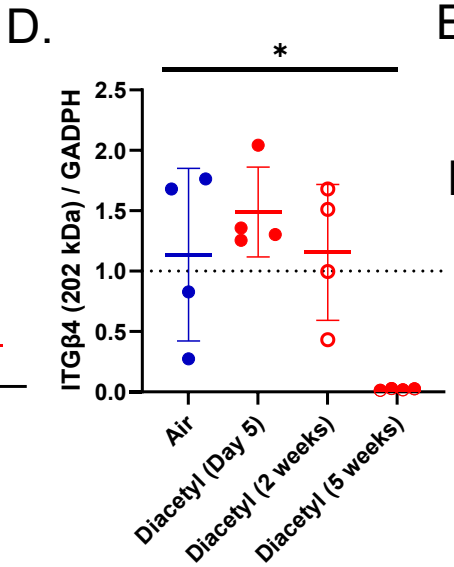
D.
ITGβ4 (202 kDa) / GADPH
2.5
2.0
1.5
1.0
0.5
0.0
*
Air
Diacetyl (Day 5)
Diacetyl (2 weeks)
Diacetyl (5 weeks)

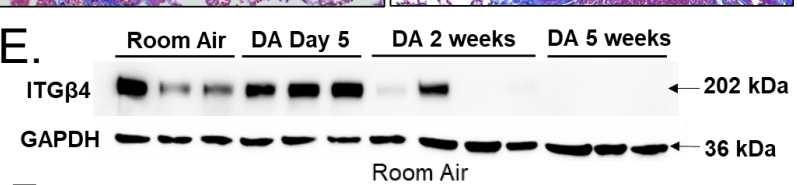
E.
Room Air
DA Day 5
DA 2 weeks
DA 5 weeks
ITGβ4
GAPDH
202 kDa
36 kDa
Room Air

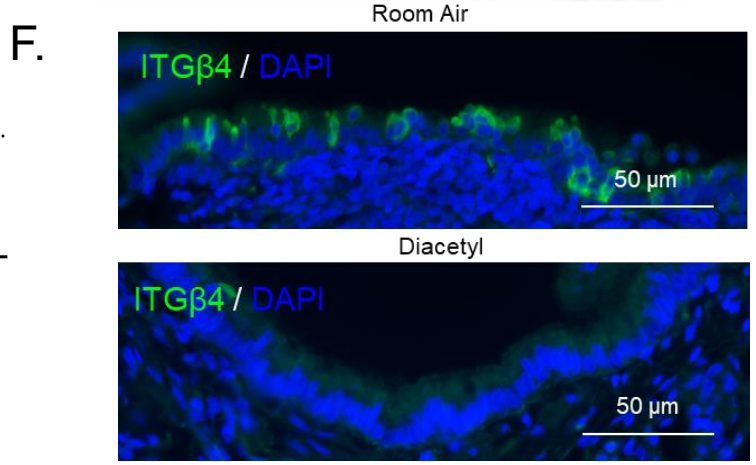
F.
ITGβ4 / DAPI
50 µm
Diacetyl
ITGβ4 / DAPI
50 µm

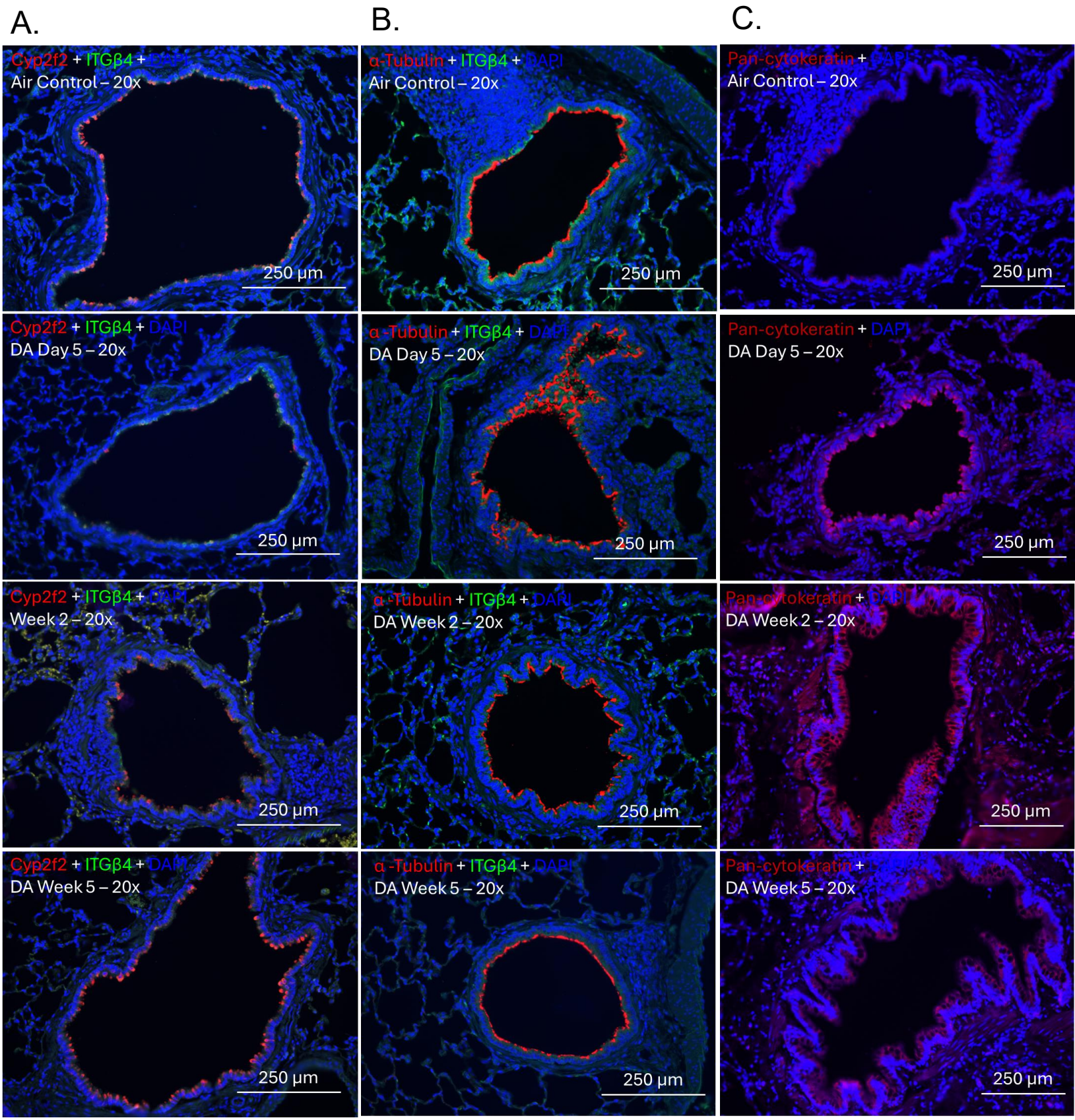
A.
B.
C.
Cyp2f2 + ITGβ4 + DAPI
Air Control – 20x
α-Tubulin + ITGβ4 + DAPI
Air Control – 20x
Pan-cytokeratin + DAPI
Air Control – 20x
Cyp2f2 + ITGβ4 + DAPI
DA Day 5 – 20x
α-Tubulin + ITGβ4 + DAPI
DA Day 5 – 20x
Pan-cytokeratin + DAPI
DA Day 5 – 20x
Cyp2f2 + ITGβ4 + DAPI
Week 2 – 20x
α-Tubulin + ITGβ4 + DAPI
DA Week 2 – 20x
Pan-cytokeratin + DAPI
DA Week 2 – 20x
Cyp2f2 + ITGβ4 + DAPI
DA Week 5 – 20x
α-Tubulin + ITGβ4 + DAPI
DA Week 5 – 20x
Pan-cytokeratin + DAPI
DA Week 5 – 20x
250 µm

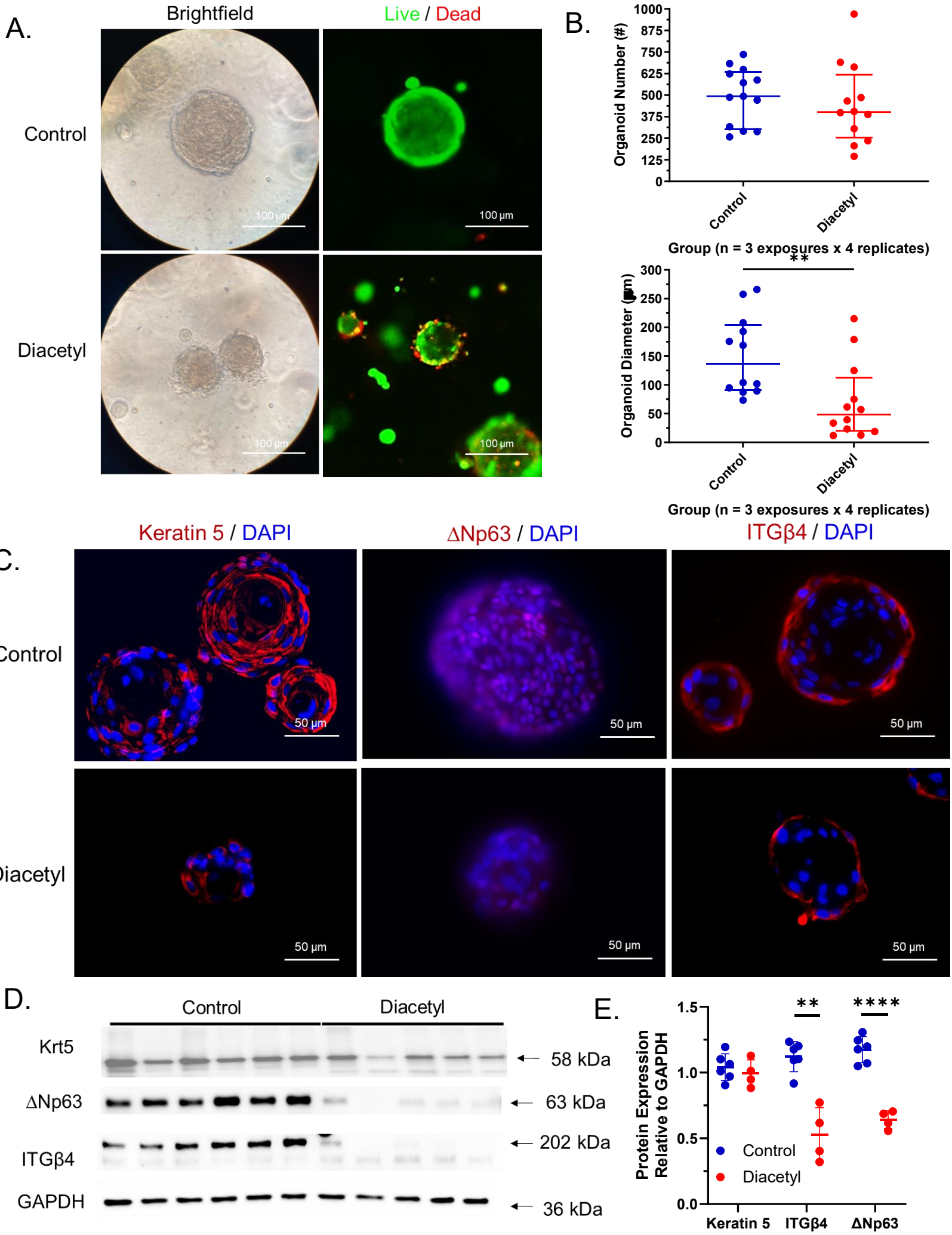
A.
Brightfield
Live / Dead
Control
Diacetyl
100 µm
B.
Organoid Number (#)
1000
875
750
625
500
375
250
125
0
Control
Diacetyl
Group (n = 3 exposures x 4 replicates)
**
Organoid Diameter (µm)
300
250
200
150
100
50
0
Control
Diacetyl
Group (n = 3 exposures x 4 replicates)
C.
Keratin 5 / DAPI
ΔNp63 / DAPI
ITGβ4 / DAPI
Control
Diacetyl
50 µm
D.
Control
Diacetyl
Krt5
ΔNp63
ITGβ4
GAPDH
58 kDa
63 kDa
202 kDa
36 kDa
E.
Protein Expression Relative to GAPDH
1.5
1.0
0.5
0.0
**
****
Control
Diacetyl
Keratin 5
ITGβ4
ΔNp63

A.

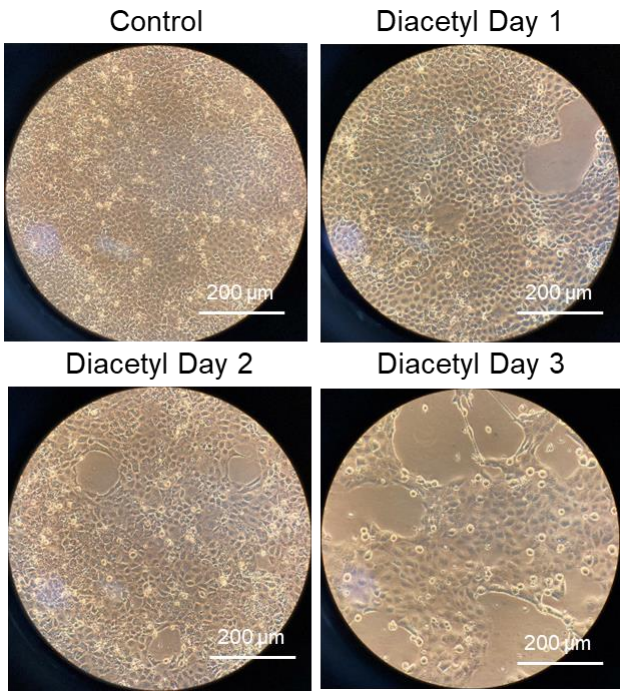
Control
Diacetyl Day 1
Diacetyl Day 2
Diacetyl Day 3
200 µm
200 µm
200 µm
200 µm

B.

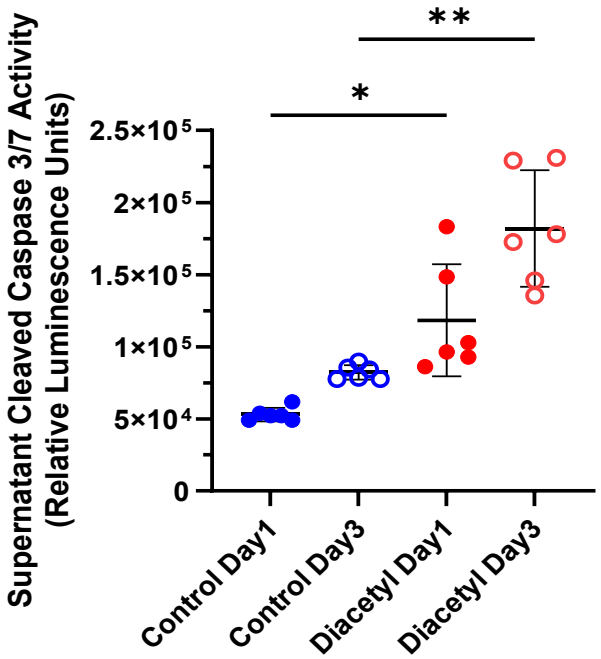
**
*
Supernatant Cleaved Caspase 3/7 Activity (Relative Luminescence Units)
2.5×10⁵
2×10⁵
1.5×10⁵
1×10⁵
5×10⁴
0
Control Day1
Control Day3
Diacetyl Day1
Diacetyl Day3

C.

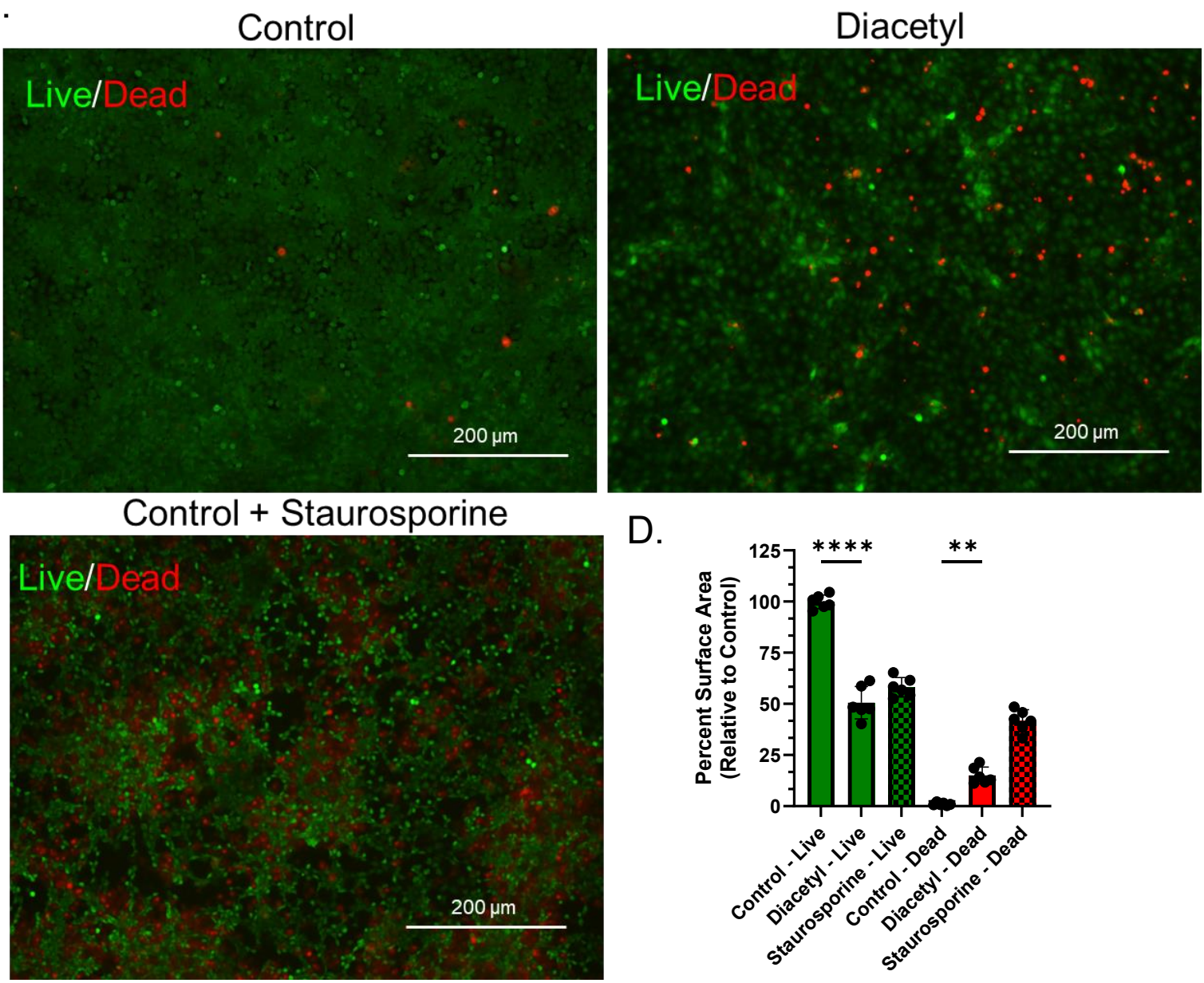
Control
Live/Dead
200 µm
Diacetyl
Live/Dead
200 µm
Control + Staurosporine
Live/Dead
200 µm

D.

****
**
Percent Surface Area (Relative to Control)
125
100
75
50
25
0
Control - Live
Diacetyl - Live
Staurosporine - Live
Control - Dead
Diacetyl - Dead
Staurosporine - Dead

A.

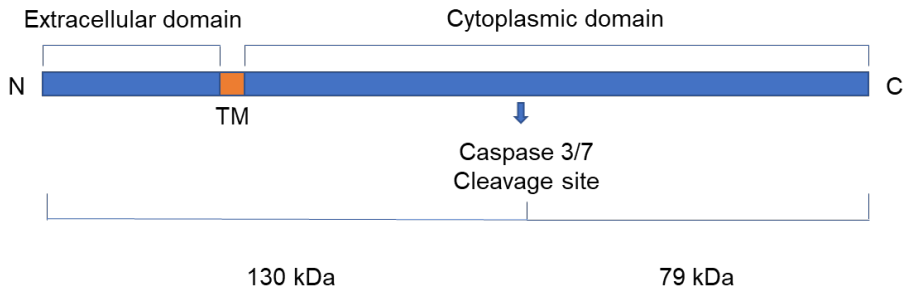
Extracellular domain
Cytoplasmic domain
N
C
TM
Caspase 3/7
Cleavage site
130 kDa
79 kDa

B.

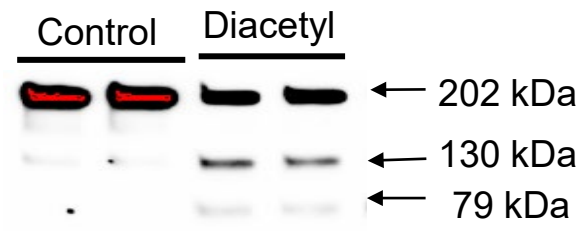
Control
Diacetyl
202 kDa
130 kDa
79 kDa

C.

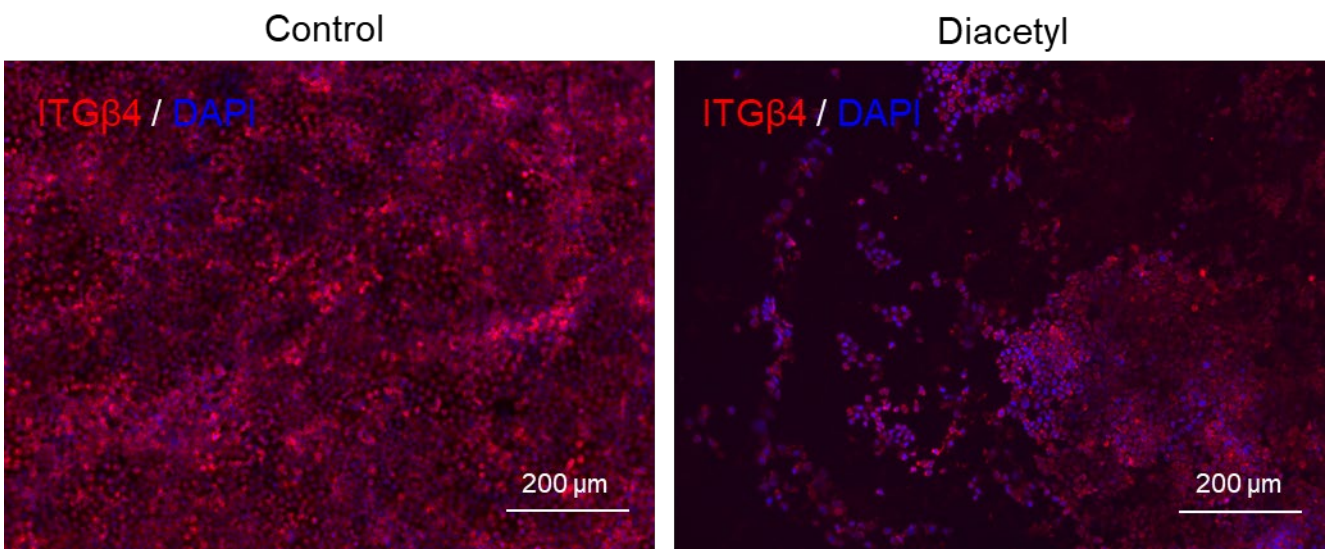
Control
Diacetyl
ITGβ4 / DAPI
ITGβ4 / DAPI
200 μm
200 μm

D.

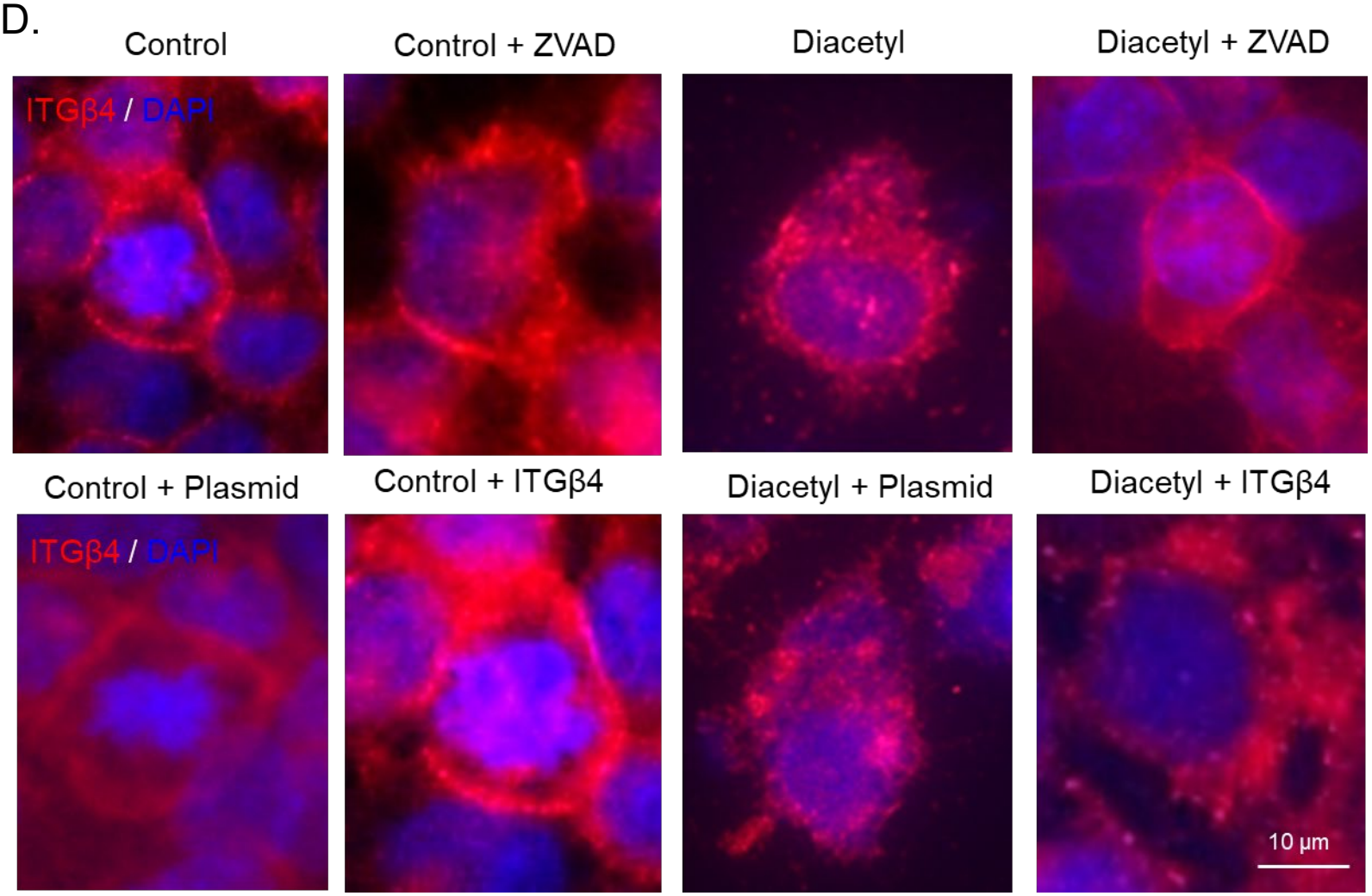
Control
Control + ZVAD
Diacetyl
Diacetyl + ZVAD
ITGβ4 / DAPI
Control + Plasmid
Control + ITGβ4
Diacetyl + Plasmid
Diacetyl + ITGβ4
ITGβ4 / DAPI
10 μm

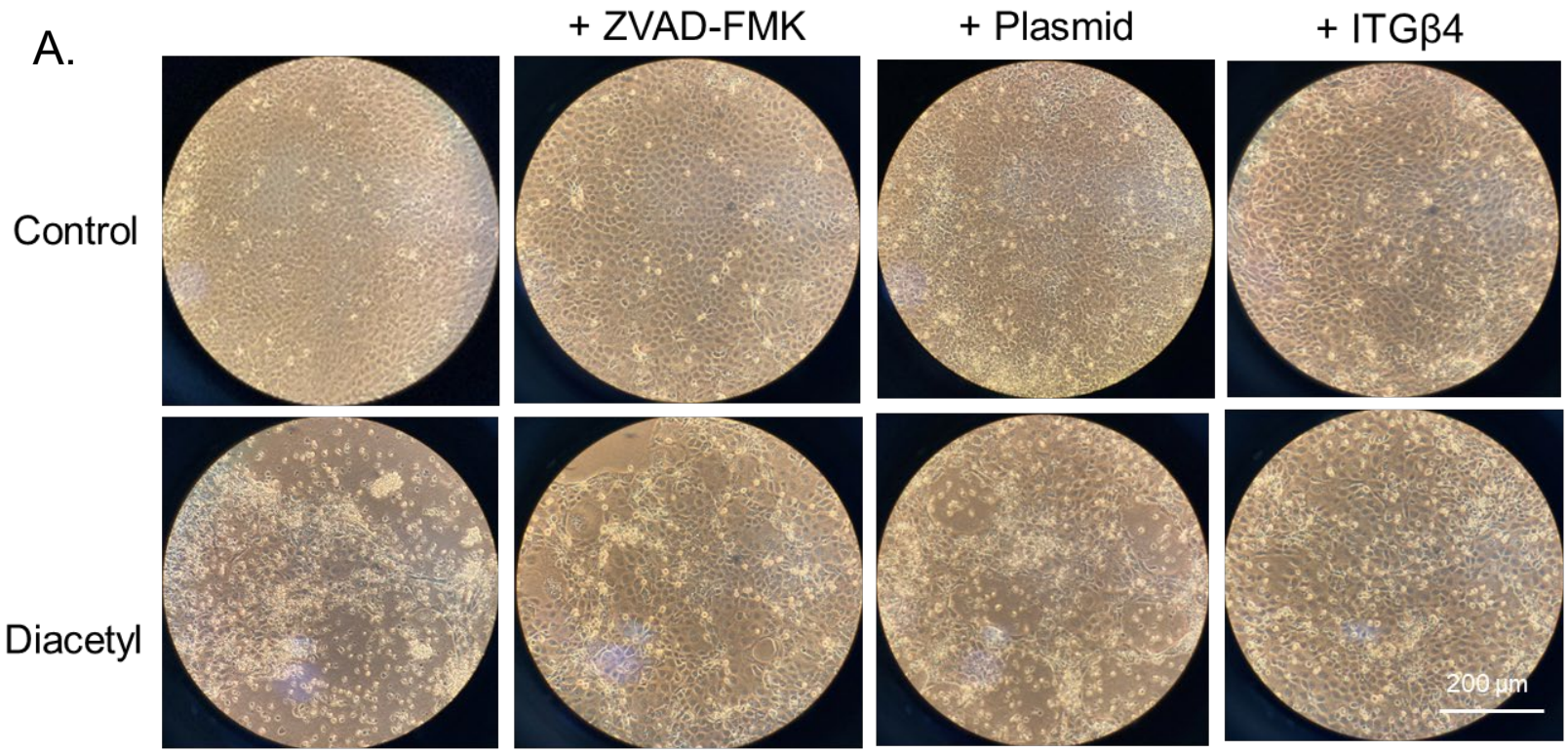
A.
+ ZVAD-FMK
+ Plasmid
+ ITGβ4
Control
Diacetyl
200 μm

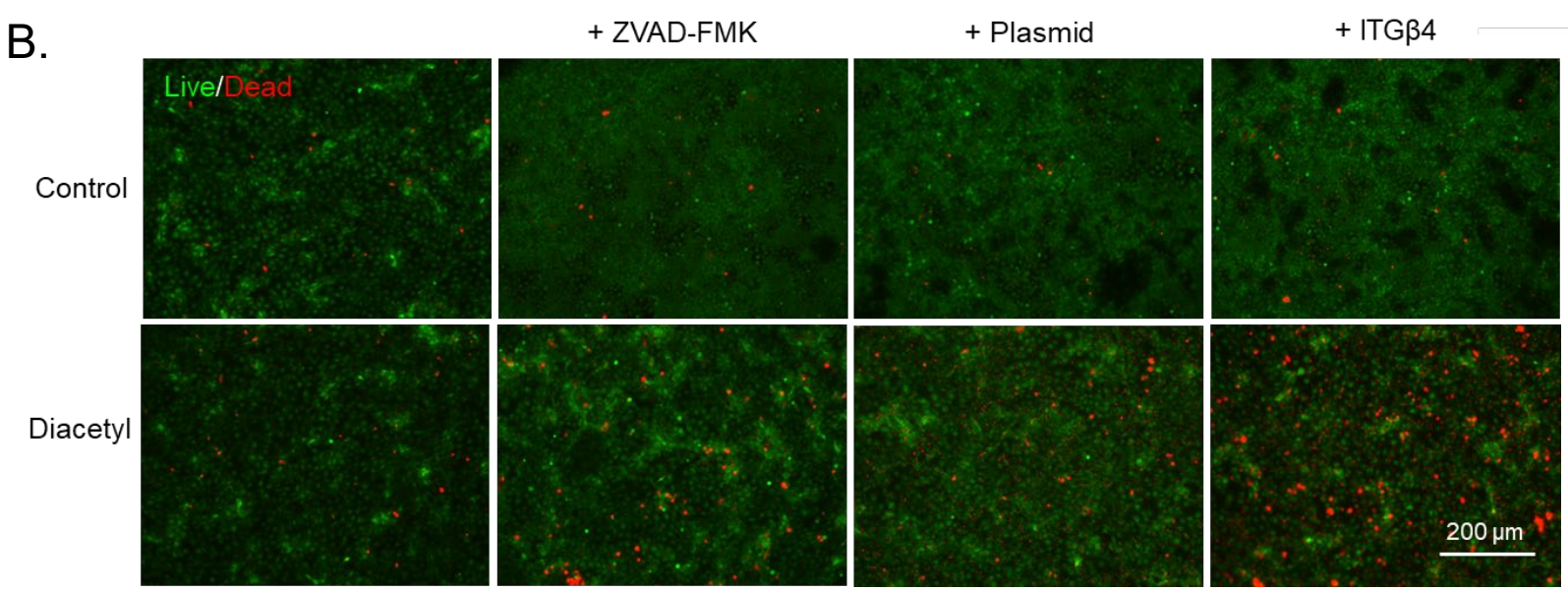
B.
+ ZVAD-FMK
+ Plasmid
+ ITGβ4
Live/Dead
Control
Diacetyl
200 μm

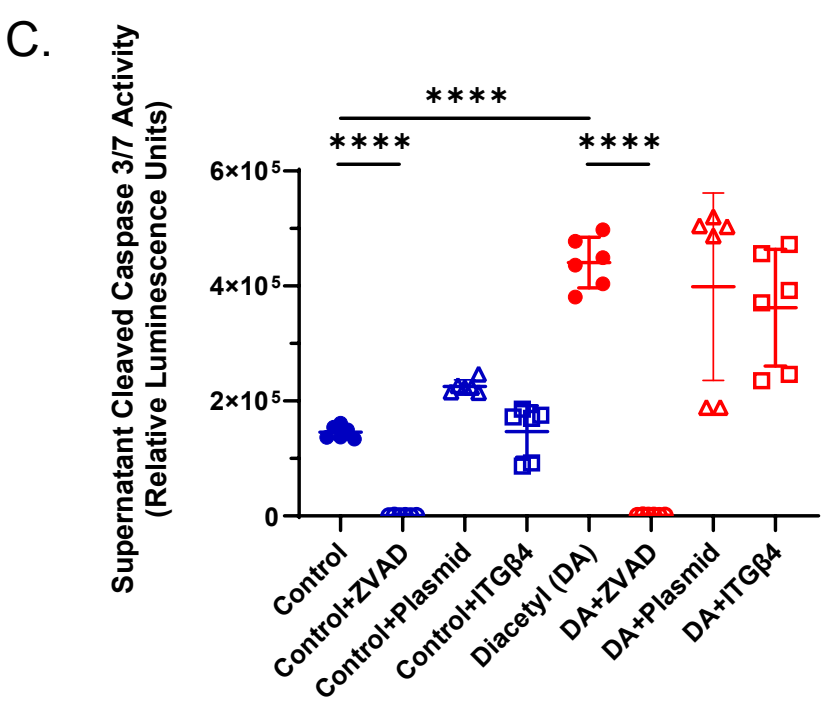
C.
Supernatant Cleaved Caspase 3/7 Activity (Relative Luminescence Units)
****
****
****
6×10⁵
4×10⁵
2×10⁵
0
Control
Control+ZVAD
Control+Plasmid
Control+ITGβ4
Diacetyl (DA)
DA+ZVAD
DA+Plasmid
DA+ITGβ4

A.

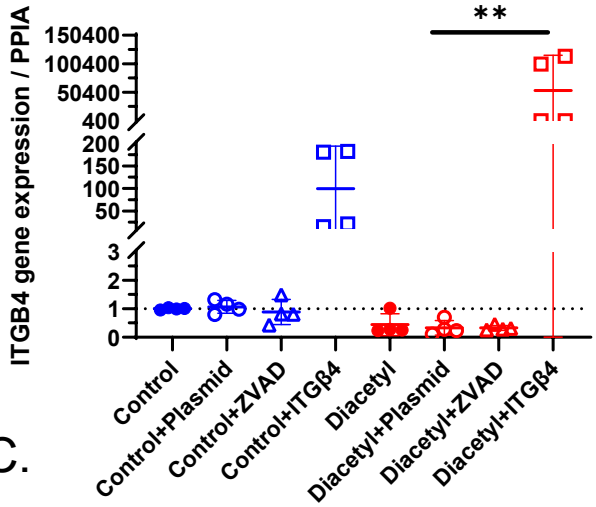
ITGB4 gene expression / PPIA
**
Control
Control+Plasmid
Control+ZVAD
Control+ITGβ4
Diacetyl
Diacetyl+Plasmid
Diacetyl+ZVAD
Diacetyl+ITGβ4

B.

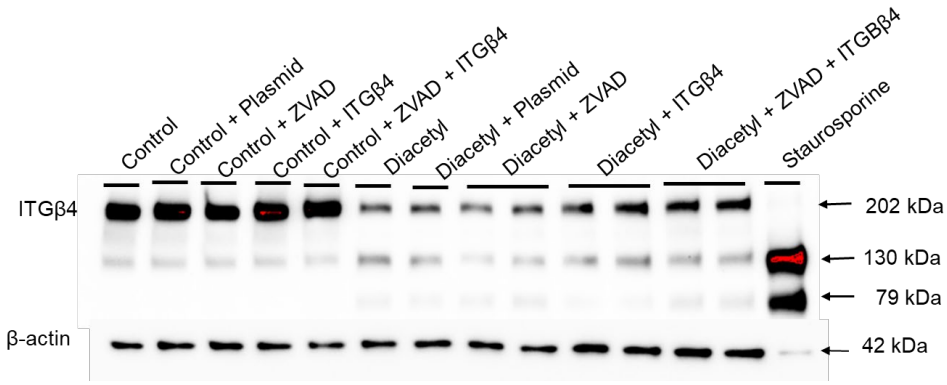
Control
Control + Plasmid
Control + ZVAD
Control + ITGβ4
Control + ZVAD + ITGβ4
Diacetyl
Diacetyl + Plasmid
Diacetyl + ZVAD
Diacetyl + ITGβ4
Diacetyl + ZVAD + ITGBβ4
Staurosporine
ITGβ4
β-actin
202 kDa
130 kDa
79 kDa
42 kDa

C.

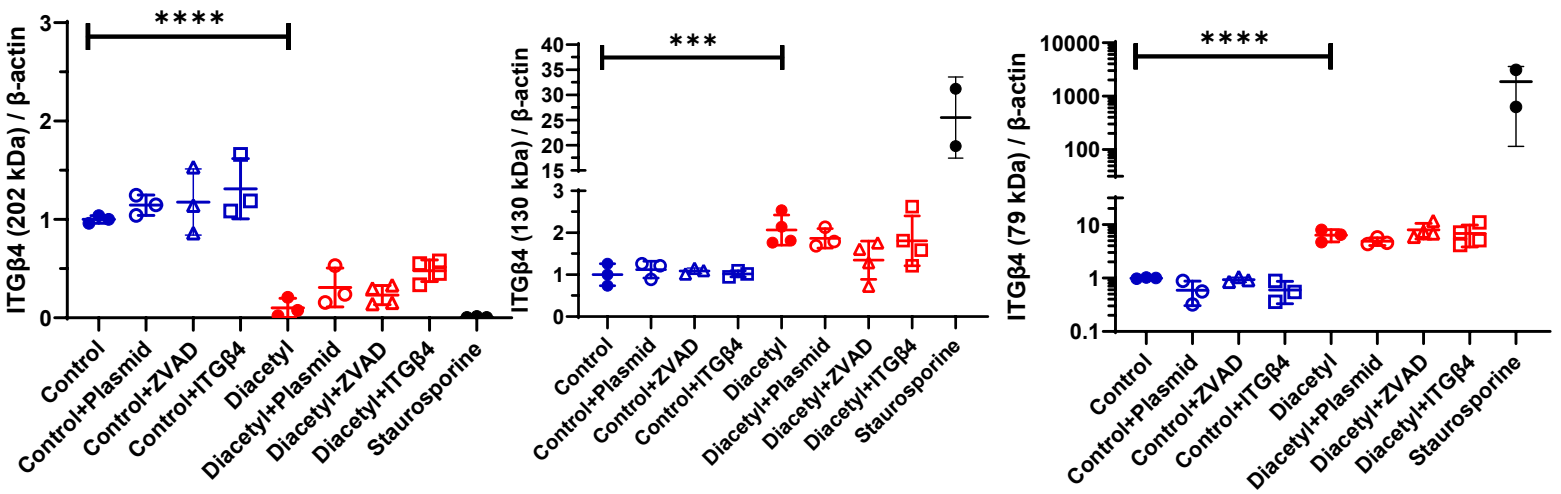
ITGβ4 (202 kDa) / β-actin
****
ITGβ4 (130 kDa) / β-actin
***
ITGβ4 (79 kDa) / β-actin
****
Control
Control+Plasmid
Control+ZVAD
Control+ITGβ4
Diacetyl
Diacetyl+Plasmid
Diacetyl+ZVAD
Diacetyl+ITGβ4
Staurosporine

D.

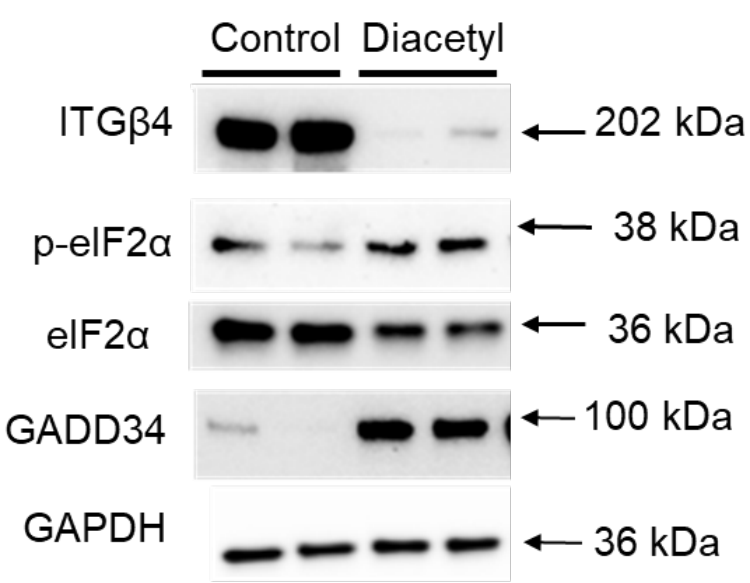
Control
Diacetyl
ITGβ4
202 kDa
p-eIF2α
38 kDa
eIF2α
36 kDa
GADD34
100 kDa
GAPDH
36 kDa

E.

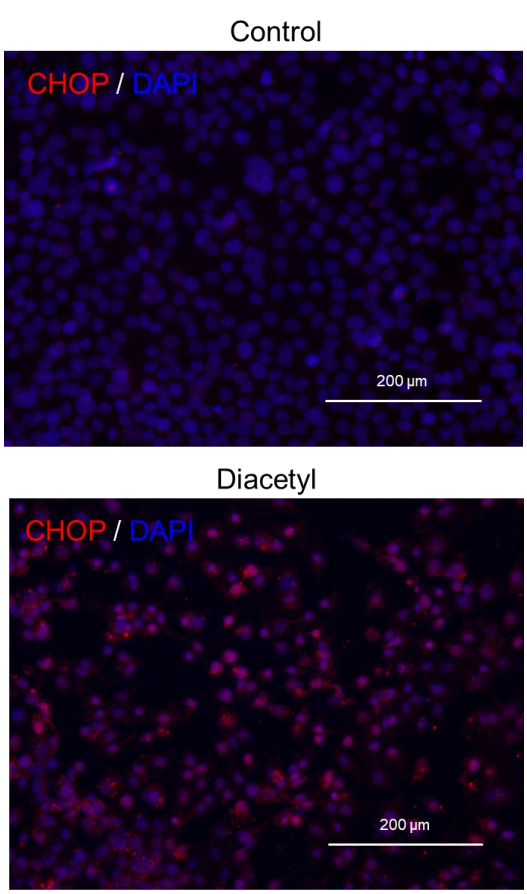
Control
CHOP / DAPI
200 μm
Diacetyl
CHOP / DAPI
200 μm